Asymmetric lysosome inheritance predicts hematopoietic stem cell activation

Authors: Dirk Loeffler[1,2], Arne Wehling[1], Florin Schneiter[1], Yang Zhang[1], Niklas Müller-Bötticher[1], Philipp S. Hoppe[1,2], Oliver Hilsenbeck[1,2], Konstantinos D. Kokkaliaris[1,2], Max Endele[1,2], Timm Schroeder[1,2]*.

Affiliations:

[1]Department of Biosystems Science and Engineering, ETH Zurich, Basel, Switzerland

[2]Research unit Stem Cell Dynamics, Helmholtz Center Munich - German Research Center for Environmental Health (GmbH), Neuherberg, Germany

* Correspondence to: Timm Schroeder, Department of Biosystems Science and Engineering, Eidgenössische Technische Hochschule Zurich, Mattenstrasse 26, 4058 Basel, Switzerland; e-mail: timm.schroeder@bsse.ethz.ch.

15 Hematopoietic stem cells (HSCs) self-renew and differentiate into all blood lineages lifelong and
16 can repair damaged blood systems upon transplantation. Asymmetric cell division (ACD) has been
17 suspected as a regulator of HSC fates, but its existence could never be shown directly[1]. In ACD,
18 asymmetric future daughter cell fates are prospectively determined by a mechanism linked to
19 mitosis. This can be mediated by asymmetric inheritance of cell-extrinsic niche signals by e.g.
20 orienting the divisional plane, or by asymmetric inheritance of cell-intrinsic fate determinants.
21 Importantly, neither the observation of asymmetric inheritance alone, nor of asymmetric daughter
22 fates alone are sufficient to demonstrate ACD[2]. In both cases, sister fates could be controlled by
23 division-independent mechanisms. Here, we demonstrate that the cellular degradative machinery
24 including lysosomes, autophagosomes, mitophagosomes and NUMB can be asymmetrically
25 inherited into HSC daughters. This asymmetric inheritance predicts asymmetric future metabolic
26 and translational activation and fates of HSC daughters and their offspring. Hence, we provide
27 first evidence for the existence of HSC asymmetric cell division.
28
29
30 Previous attempts to demonstrate HSC ACD relied on either only asymmetric daughter cell fates
31 acquired after division, or only the asymmetric inheritance of fate determinants during division[1,3–
32 6]. NUMB[3,5], AP2A2[4], TIE2[6], CD63[7] CDC42[8] and active mitochondria[9] were suggested to be
33 asymmetrically inherited during HSC divisions. However, e.g. CD63 and NUMB were only
34 analyzed in fixed hematopoietic progenitor (not stem) cells[3,5,7], different live reporters yielded
35 different results[4,5], and non-mitotic and/or non-related cells might have been mistaken for paired
36 daughters[3,5]. It thus remained unclear whether NUMB is actually asymmetrically inherited during

37 HSC divisions. In addition, no correlation with future daughter cells fates, and thus functional
38 relevance of a potential asymmetric inheritance, could be demonstrated.
39 Here, we used quantitative long-term live single-cell imaging and tracking[10–15] to combine
40 molecular quantification during HSC division with future cell-fate quantification of daughter cells.
41 First, we expressed fluorescent protein fusions of 13 candidates in murine HSCs (Supplementary
42 Data Fig. 1) and quantified their inheritance during HSC division *in vitro* (Fig. 1, Extended Data
43 Fig. 1). Importantly, since daughter cells can quickly adopt differences in reporter gene expression
44 after mitosis (Extended Data Figs. 1d, e), we quantified inheritance directly after division
45 (Extended Data Fig. 1). Only CD63VENUS and mCherryNUMB but not NUMBVENUS showed
46 clear asymmetric inheritance (Figs. 1b, c, Extended Data Fig. 1, Videos S1-2)). We therefore
47 analyzed the inheritance also of endogenous NUMB in fixed mitotic cKIT+Sca1+lineage- cells
48 (KSL). In contrast to previous reports suggesting several-fold differences of inherited NUMB
49 between sister cells[5,16], we found NUMB sister ratios to rarely exceeded 2-fold (Extended Data
50 Figs. 2a-d). They were also highest in cells with lower signal over background (Extended Data
51 Fig. 2d), thus possibly only resembling random noise effects without functional relevance.
52 However, daughters receiving more NUMB also received more AP2A2[4] and PARD3b (Extended
53 Data Figs. 2e-k), suggesting that these small daughter cell differences are not just random and
54 might be functionally relevant.
55 Since previous NUMB reporters yielded different observations, we quantified the colocalization
56 of endogenous NUMB with NUMBVENUS and mCherryNUMB in 3D. While endogenous
57 NUMB and mCherryNUMB were mostly localized in vesicles, NUMBVENUS localized at the
58 plasma membrane (Extended Data Figs. 2l, m) revealing that mCherryNUMB is the more faithful
59 reporter (Extended Data Figs. 2n, o). While we found clear asymmetric mCherryNUMB

60 inheritance during HSC divisions (Figs. 1b, c, Videos S1-2), cocultures on 7F2 (17.2±3.1%) did
61 not, in contrast to a previous report[3], increase asymmetry frequencies over OP9 (19.5±1.3%)
62 stroma (Fig. 1d).
63 To identify markers for asymmetric daughter fates, we quantified the expression dynamics of Sca1,
64 CD105, CD41, CD48 and CD71 (Figs. 1e, f). Clustering of paired daughter cell dynamics yielded
65 three distinct behaviors (symmetric, weakly- and asymmetric) for Sca1, CD48, CD41 and CD71,
66 and two for CD105 (Fig. 1f). Interestingly, the frequencies of a-/symmetric daughter fates varied
67 between the differentiation markers (Fig. 1f).
68 We next tested whether asymmetric mCherryNUMB inheritance can predict asymmetric future
69 HSC daughter fates. Sisters with symmetric mCherryNUMB inheritance showed symmetric and
70 asymmetric expression dynamics for all markers, while Sca1 was mostly expressed symmetrically
71 (Figs. 2a-d, Extended Data Fig. 3). In contrast, sisters with asymmetric inheritance showed an
72 increased frequency of asymmetric Sca1, CD105 and CD71 expression (Figs. 2a-d, Extended Data
73 Figs. 3d, e). In addition, increased production of CD48, CD105 and CD71, but not CD41 and Sca1
74 was observed in daughter cells receiving less mCherryNUMB (Extended Data Fig. 3c). CD48 and
75 CD71 upregulation has been associated with differentiation[17] and activation[18], while elevated Sca1
76 levels indicate less differentiated cells[17], suggesting that HSC daughters receiving less
77 mCherryNUMB are metabolically activated and induced to differentiate.
78 Following this hypothesis, other markers for HSC activation and differentiation should also
79 correlate with CD71. Mitochondrial activation[19], reactive oxygen species (ROS) production[20] and
80 c-MYC upregulation are indicators of HSC activation, exhaustion and differentiation[21,22], while
81 low mitochondrial activity and clearance are crucial for HSC function[6,19]. Probes for mitochondrial
82 activation like Tetramethylrhodamine (TMRM) have been demonstrated to be a faithful reporter

83 for functional HSCs in vitro[9,19]. Using a GFP-c-MYC reporter mouse[23], we quantified the
84 expression kinetics of CD71, GFP-c-MYC, TMRM[9,19] or ROS levels using CellROX dyes in
85 dividing HSCs and their daughters (Figs. 2e-g, Extended Data Fig. 4).
86 As expected, HSCs are metabolically inactive and express low levels of CD71, GFP-c-MYC,
87 TMRM and ROS (Extended Data Figs. 4a, b-d left panels). In HSC daughter cells, GFP-c-MYC,
88 TMRM and ROS expression levels strongly correlated with the upregulation of CD71 (Figs. 2e-g,
89 Extended Data Figs. 4a-d right panels). When both HSC daughter cells upregulated CD71, the
90 levels of GFP-c-MYC, TMRM and ROS increased also in both daughters (Figs. 2e-g, Extended
91 Data Figs. 4f-g). When only one sister upregulated CD71, as after asymmetric inheritance of
92 NUMB, the levels of GFP-c-MYC, TMRM and ROS increased in the same sister but remained
93 low in the other (Figs. 2e-g). Further differentiated MPP1-5s have higher levels of GFP-c-MYC
94 and upregulate CD71, GFP-c-MYC, TMRM and ROS faster than HSCs (Extended Data Fig. 4e-
95 l), confirming their upregulation as a differentiation or activation marker. In contrast, CD105 and
96 Sca1, which both are highly expressed on HSCs and lost upon differentiation, are downregulated
97 after CD71 upregulation but not in CD71 low cells (Extended Data Figs. 4m-p). GFP-c-MYC and
98 TMRM are upregulated about 2-3h prior to CD71, while ROS levels increase with CD71 (Figs.
99 2h, i). These observations demonstrate that HSC daughters receiving less mCherryNUMB get
100 metabolically activated and suggest c-MYC upregulation and mitochondria activation as early
101 ACD effectors, then inducing CD71, ROS production and differentiation.
102 Since both asymmetrically inherited proteins, NUMB and CD63 (Extended Data Figs. 1a-d and[24])
103 have been associated with lysosomes[25,26] we speculated that lysosomes might be asymmetrically
104 inherited. In this case, NUMB´s asymmetry might only reflect its lysosomal localization. We found
105 clear asymmetric inheritance of the lysosomal marker LAMP1VENUS (Extended Data Figs. 5a-

106 c) and of the pH sensitive fluorescent lysosome reporter probe LysoBrite in HSC daughters (Figs.
107 3a-c, Extended Data Figs. 5e-g), and of LAMP2 in fixed mitotic KSL (Extended Data Fig. 5d),
108 showing asymmetric lysosomes inheritance. Like for mCherryNUMB, asymmetric lysosome
109 inheritance predicts onsets of CD71, CD48 and CD105 in HSC daughters (Figs. 3a-c, Extended
110 Data Figs. 5g-i) but not of CD41 and Sca1, suggesting a common mechanism underlying both
111 NUMB and lysosome asymmetries. Indeed, LAMP2+ lysosomes are asymmetrically co-inherited
112 into the same KSL daughter cell as endogenous NUMB (Extended Data Figs. 6a-e), and 15±2%
113 of endogenous NUMB and 48±2.5% of mCherryNUMB colocalize with LAMP2 (Extended Data
114 Figs. 6f-h). In living HSCs, mCherryNUMB and lysosomes also co-localize partially, and are
115 asymmetrically co-inherited into the same daughter cell (Extended Data Figs. 6i-k). NOTCH1 is
116 also asymmetrically co-inherited with lysosomes (Extended Data Figs. 5j, k), suggesting that
117 asymmetric NUMB and lysosome inheritance might act in concert to modulate NOTCH signaling
118 in one HSC daughter.
119 This suggests that daughter fate bifurcations are controlled by asymmetric lysosome inheritance.
120 Interestingly, autophagy and mitochondrial clearance are lysosome-dependent processes, and
121 required for HSC function and quiescence[6,27,28]. The asymmetric inheritance of old mitochondria
122 was reported in a mammary cell line, but no asymmetric inheritance of lysosomes or
123 autophagosomes was found[29]. To test whether autophagosomes and mitophagosomes are
124 asymmetrically inherited in HSCs, we quantified LC3β, TOMM20 and LAMP1 in mitotic HSCs.
125 We found asymmetric co-inheritance of autophagosomes, mitophagosomes and lysosomes (Fig.
126 3d). In living HSCs, a double fluorescence reporter which, due to differences in maturation time
127 and pH stability can be used to identify nascent, mature or degrading proteins[30], confirmed these
128 results (Extended Data Figs. 7a-c).

129 If asymmetrically inherited lysosomes maintain a metabolically inactive cell, the sister receiving
130 less of the lysosomal degradative machinery should also increase in translational activity.
131 Asymmetric translational activity of HSC daughters increases with cell cycle progression
132 (Extended Data Figs. 8a-c), prior to CD71 upregulation (Extended Data Fig. 8d), and indeed
133 correlates with CD71 and lysosomal asymmetry (Extended Data Figs. 8e, f).
134 Next, we tested whether this asymmetry predicts long-term fates of the progeny of HSC daughters.
135 Asymmetric lysosome inheritance correlated with higher overall heterogeneity during long-term
136 differentiation (Fig. 4d), but without a bias for specific lineages (Extended Data Fig. 9,
137 Supplementary Data Fig. 2). This was further confirmed by continuous long-term single-cell
138 quantification of HSCs and their progeny over 5 generations by clustering of single-cell dynamics
139 (e.g. of differentiation markers Sca1, CD41, FcγR), and fate trajectories in tracked lineage trees
140 (Figs. 4a-d, Extended Data Fig. 9). Asymmetric lysosome inheritance predicted asymmetric
141 differentiation progression of HSC daughters (Fig. 4c), with lysosome low HSC daughters being
142 induced to differentiate without inducing specific lineage choices (Fig. 4). These may be made,
143 independently of differentiation induction, in a specific time window after every mitosis.
144 Alternatively, culture conditions could dominate over ACD in inducing differentiation, thus
145 homogenizing lineage output after ACD in culture.
146 Taken together, we show that lysosomes, autophagosomes, mitophagosomes, NOTCH1, CD63
147 and NUMB are asymmetrically inherited by HSC daughters, and functionally predict the
148 metabolic, translational and differentiation activation in HSC daughter cells, and the increased
149 heterogeneity of their long-term progeny. The used HSC purification approach yields a population
150 with ~30-50%[21,22] purity of functional HSCs, leaving the possibility that the 20-30% ACDs occur
151 outside the HSC fraction. However, we found about half of ACDs in cells with very late (> 40h)

152 first divisions, an exclusive property of functional HSCs[21]. Interestingly, while differing HSC
153 daughter fates are frequent also in the absence of ACD, ACD seems to dictate the coordinated
154 directionality of asymmetric daughter inheritance and fate acquisition. We suggest that the
155 asymmetric inheritance of the autophagosomal / lysosomal degradative machinery is involved in
156 HSC fate decisions by regulating mitochondrial clearance, autophagy and possibly NOTCH
157 signaling (Extended Data Fig. 10) and provide the first direct experimental proof for ACD of HSCs
158 *in vitro*.
159
160 **References:**

161 1. Pham, K., Sacirbegovic, F. & Russell, S. M. Polarized cells, polarized views: Asymmetric
162 cell division in hematopoietic cells. *Front. Immunol.* **5**, 1–14 (2014).
163 2. Horvitz, H. R. & Herskowitz, I. Mechanisms of asymmetric cell division: two Bs or not
164 two Bs, that is the question. *Cell* **68**, 237–55 (1992).
165 3. Wu, M. *et al.* Imaging hematopoietic precursor division in real time. *Cell Stem Cell* **1**,
166 541–54 (2007).
167 4. Ting, S. B. *et al.* Asymmetric segregation and self-renewal of hematopoietic stem and
168 progenitor cells with endocytic Ap2a2. *Blood* **119**, 2510–2522 (2012).
169 5. Zimdahl, B. *et al.* Lis1 regulates asymmetric division in hematopoietic stem cells and in
170 leukemia. *Nat. Genet.* **46**, 245–52 (2014).
171 6. Ito, K. *et al.* Self-renewal of a purified Tie2+hematopoietic stem cell population relies on
172 mitochondrial clearance. *Science (80-.).* **354**, 1156–1160 (2016).
173 7. Beckmann, J., Scheitza, S., Wernet, P., Fischer, J. C. & Giebel, B. Asymmetric cell
174 division within the human hematopoietic stem and progenitor cell compartment:
175 Identification of asymmetrically segregating proteins. *Blood* **109**, 5494–5501 (2007).

176 8. Florian, M. C. *et al.* Cdc42 Activity Regulates Hematopoietic Stem Cell Aging and
177 Rejuvenation. *Cell Stem Cell* **10**, 520–530 (2012).
178 9. Vannini, N. *et al.* The NAD-Booster Nicotinamide Riboside Potently Stimulates
179 Hematopoiesis through Increased Mitochondrial Clearance. *Cell Stem Cell* **24**, 405-418.e7
180 (2019).
181 10. Hoppe, P. S. *et al.* Early myeloid lineage choice is not initiated by random PU.1 to
182 GATA1 protein ratios. *Nature* **535**, 299–302 (2016).
183 11. Hilsenbeck, O. *et al.* Software tools for single-cell tracking and quantification of cellular
184 and molecular properties. *Nat Biotech* **34**, 703–706 (2016).
185 12. Loeffler, D. *et al.* Mouse and human HSPC immobilization in liquid culture by CD43 or
186 CD44-antibody coating. *Blood* **131**, 1425–1429 (2018).
187 13. Loeffler, D. & Schroeder, T. Understanding cell fate control by continuous single-cell
188 quantification. *Blood* **133**, 1406–1414 (2019).
189 14. Skylaki, S., Hilsenbeck, O. & Schroeder, T. Challenges in long-term imaging and
190 quantification of single-cell dynamics. *Nat. Biotechnol.* **34**, 1137–1144 (2016).
191 15. Eilken, H. M., Nishikawa, S.-I. & Schroeder, T. Continuous single-cell imaging of blood
192 generation from haemogenic endothelium. *Nature* **457**, 896–900 (2009).
193 16. Schroeder, T. Asymmetric Cell Division in Normal and Malignant Hematopoietic
194 Precursor Cells. *Cell Stem Cell* **1**, 479–481 (2007).
195 17. Zhang, C. C. & Lodish, H. F. Murine hematopoietic stem cells change their surface
196 phenotype during ex vivo expansion. *Blood* **105**, 4314–20 (2005).
197 18. Motamedi, M., Xu, L. & Elahi, S. Correlation of transferrin receptor (CD71) with Ki67
198 expression on stimulated human and mouse T cells: The kinetics of expression of T cell

199 activation markers. *J. Immunol. Methods* **437**, 43–52 (2016).

200 19. Vannini, N. *et al.* Specification of haematopoietic stem cell fate via modulation of
201 mitochondrial activity. *Nat. Commun.* **7**, 1–9 (2016).

202 20. Ito, K. *et al.* Reactive oxygen species act through p38 MAPK to limit the lifespan of
203 hematopoietic stem cells. *Nat. Med.* **12**, 446–451 (2006).

204 21. Cabezas-Wallscheid, N. *et al.* Vitamin A-Retinoic Acid Signaling Regulates
205 Hematopoietic Stem Cell Dormancy. *Cell* **169**, 807-823.e19 (2017).

206 22. Wilson, A. *et al.* Hematopoietic stem cells reversibly switch from dormancy to self-
207 renewal during homeostasis and repair. *Cell* **135**, 1118–29 (2008).

208 23. Huang, C. Y., Bredemeyer, A. L., Walker, L. M., Bassing, C. H. & Sleckman, B. P.
209 Dynamic regulation of c-Myc proto-oncogene expression during lymphocyte development
210 revealed by a GFP-c-Myc knock-in mouse. *Eur. J. Immunol.* **38**, 342–349 (2008).

211 24. Pols, M. S. & Klumperman, J. Trafficking and function of the tetraspanin CD63. *Exp. Cell*
212 *Res.* **315**, 1584–1592 (2009).

213 25. Shao, X. *et al.* Mammalian Numb protein antagonizes Notch by controlling postendocytic
214 trafficking of the Notch ligand Delta-like 4. *J. Biol. Chem.* **292**, 20628–20643 (2017).

215 26. McGill, M. A., Dho, S. E., Weinmaster, G. & McGlade, C. J. Numb regulates post-
216 endocytic trafficking and degradation of notch1. *J. Biol. Chem.* **284**, 26427–26438 (2009).

217 27. Ho, T. T. *et al.* Autophagy maintains the metabolism and function of young and old stem
218 cells. *Nature* **543**, 205–210 (2017).

219 28. Warr, M. R. *et al.* FOXO3A directs a protective autophagy program in haematopoietic
220 stem cells. *Nature* **494**, 323–327 (2013).

221 29. Katajisto, P. *et al.* Asymmetric apportioning of aged mitochondria between daughter cells

222 is required for stemness. *Science (80-.).* **348**, 340–343 (2015).

223 30. Kimura, S., Noda, T. & Yoshimori, T. Dissection of the autophagosome maturation
224 process by a novel reporter protein, tandem fluorescent-tagged LC3. *Autophagy* **3**, 452–60
225 (2007).

226

227 **Supplementary Information** is linked to the online version of the paper at
228 www.nature.com/nature.

229

230 **Acknowledgments** We are grateful to S. Ammersdoerfer, G. Camenisch, MD. Hussherr, V.
231 Jäggin, T. Lopes, H. Oller, C. Raithel, B. Vogel and A. Ziegler for technical support. This work
232 was supported by DFG SFB 684 and the SNF to T.S. T.S. and O.H. acknowledge financial
233 support from SystemsX.ch. We thank J. Arias for providing the pHLuorinDsRedLC3β cDNA.

234

235 **Author contributions** D.L. planned and performed experiments and analyzed data with A.W.,
236 F.S., Y.Z. and N.M.B.; O.H., P.S.H., M.E., K.D.K. contributed to software developments. P.S.H.
237 and M.E. provided support with flow cytometry. T.S. designed and supervised the study,
238 developed and maintained quantitative long-term bioimaging with D.L. and K.D.K. All authors
239 read and commented on the final manuscript.

240

241 **Author Information:** Reprints and permissions information is available at
242 www.nature.com/reprints

243 **Competing interests:** The authors declare no competing interests.

Correspondence and requests for materials should be addressed to timm.schroeder@bsse.ethz.ch.

Additional information

Data and materials availability: All data is available in the main text or the supplementary materials.

Extended data is available for this paper at nature.com.

253 **Figure 1 | Asymmetric mCherryNUMB inheritance and asymmetric daughter cells fates in**
254 **purified HSCs.**

255 **a,** Experiment design. **b,** Representative video frames of dividing HSCs transduced with VENUS
256 and mCherryNUMB. A- and symmetric mCherryNUMB inheritance can be observed. **c,**
257 Representative mCherryNUMB fluorescence quantification of HSC daughter cells over time for
258 a- (right) and symmetric (left) segregation during division. Fold sister differences early after
259 division are indicated. n = 3 independent experiments. **d,** Frequency of asymmetric
260 mCherryNUMB inheritance in HSCs does not differ between OP9 and 7F2 stroma co-cultures. n
261 = 5 independent experiments with 389 and 401 divisions quantified total on OP9 and 7F2,
262 respectively. mean ± SEM. Two-sided Fisher's exact test. ns = not significant. **e,** Experiment
263 design. **f,** Reliable classification of symmetric and asymmetric cell fates requires continuous
264 observation. (top) Heatmap of fluorescence dynamics over the complete life time of HSC
265 daughters. Each row represents a pair of HSC daughter cells (#1 and #2). Different degrees of
266 symmetric and asymmetric expression of Sca1 (372 analyzed cells), CD105 (382), CD48 (382),
267 CD41 (372) and CD71 (1442) between daughter cells can be clustered. (middle) Mean
268 fluorescence intensities over time of the different symmetric and asymmetric clusters of indicated
269 number of pooled time series. Mean ± SD. (bottom) Quantification of symmetric and asymmetric
270 daughter cell fate cluster frequencies. n = 6 independent experiments for Sca1, CD105, CD48,
271 CD41, n = 5 independent experiments for CD71.

272

273

Figure 2 | Asymmetric inheritance of mCherryNUMB predicts asymmetric HSC activation.

a, Experiment design. **b,** Representative video frames of HSCs with a-/symmetric mCherryNUMB inheritance. Cells with symmetric inheritance of mCherryNUMB upregulate CD71 in both daughters (grey arrow). With asymmetric inheritance, daughters receiving less mCherryNUMB upregulate CD71 (white arrow). Scale bar 10 µm. **c,** Continuous simultaneous quantification of mCherryNUMB and CD71 expression dynamics of cells shown in b. n = 3 independent experiments. **d,** Heatmap and clustering (top) and cluster frequency (bottom) of paired daughter cell CD71 dynamics. Each row represents one HSC daughter pair (#1 and #2). Daughter #1 receives more mCherryNUMB during asymmetric inheritance, which predicts CD71 upregulation. A-/ symmetric inheritance was defined as >1.8x / <1.2x mCherryNUMB sister cell ratios, respectively. (Bottom left) Mean fluorescence intensities over time of clusters 1, 2, 3 and 4 with 190, 126, 129 and 67 pooled time series, respectively. Mean ± SD. n = 3 independent experiments. **e-f,** HSC daughters upregulating CD71 also upregulate GFP-c-MYC and TMRM or ROS. In case of asymmetric CD71 onset, CD71 low daughters remain low for GFP-c-MYC, TMRM and ROS. Representative examples shown. n = 3 independent experiments. **g,** HSC daughter cell quantifications of cumulative production of CD71, GFP-c-MYC and TMRM or ROS, respectively. CD71, GFP-c-MYC and TMRM or ROS are coregulated in HSC daughters. n = 3 independent experiments with 282 and 356 daughter cells for CD71, GFP-c-MYC, TMRM and ROS, respectively. Two-sided Mann-Whitney test. **h-i,** Quantification of delay of GFP-c-MYC, TMRM and ROS upregulation in comparison to CD71, respectively. GFP-c-MYC and TMRM are upregulated prior to CD71, ROS simultaneously with CD71. n = 3, 6 and 3 independent experiments with 45, 95, 105 HSC daughter pairs for GFP-c-MYC, TMRM and ROS, respectively.

298 Two-sided Wilcoxon test. ns = not significant. Box-plot elements: center line, median; box limits,

299 upper and lower quartiles; Tukey's 1,5x interquartile range; points, outlier.

300 **Figure 3 | Lysosomes, autophagosomes and mitophagosomes are co-inherited during**
301 **asymmetric HSC divisions and predict CD71 upregulation.**

302 **a,** Video frames of HSCs with a-/symmetric LysoBrite inheritance and CD71 upregulation. Scale
303 bar 10 µm. Asymmetric inheritance of LysoBrite predicts upregulation of CD71 in the daughter
304 cell receiving less lysosomes (white arrow head). **b,** Representative examples of simultaneous
305 LysoBrite and CD71 dynamics quantification. Daughters receiving less LysoBrite later upregulate
306 CD71. n = 6 independent experiments. **c,** Heatmap and clustering (top) and cluster frequency
307 (bottom) of paired daughter cell CD71 dynamics after a-/symmetric LysoBrite inheritance. Each
308 row represents one HSC daughter pair (#1 and #2). Daughter #2 receives less LysoBrite during
309 asymmetric inheritance, which predicts CD71 upregulation. (Bottom left) Mean fluorescence
310 intensities over time of clusters 1, 2 and 3 with 157, 65 and 116 pooled time series, respectively.
311 Mean ± SD. n = 6 independent experiments. **d,** Immunostaining of mitotic purified HSCs stained
312 for TOMM20 (mitochondria), LAMP1 (lysosomes), LC3β (autophagosomes) and α-Tubulin.
313 Lysosomes, autophagosomes and mitophagosomes are asymmetrically co-inherited (bottom).
314 Asymmetric inheritance of mitophagosomes in mitotic HSCs daughter pairs (#1 and #2). n = 3
315 independent experiments, 199 mitotic HSC total. Two-sided unpaired t-test. Box-plot elements:
316 center line, median; box limits, upper and lower quartiles; Tukey's 1,5x interquartile range; points,
317 outlier. Scale bar 10 µm.

318 **Figure 4 | Asymmetric lysosome inheritance predicts HSC daughter fate heterogeneity.**

319 **a-b,** HSCs were continuously imaged with fluorescent LysoBrite, anti-Sca1, -CD41 and -FcγR for
320 5 generations. Cell fates were assigned using clustering (b) of single-cell dynamics quantification.
321 **b,** 2-dimensional representation of the HSC in vitro differentiation landscape by Uniform Manifold
322 Approximation and Projection (UMAP). Cluster localization of cells of specific generations and
323 of differentiation markers. Freshly isolated cells (generation 0) start in cluster 2 and acquire
324 different cell fates over time. n = 4 independent experiments with 11641 analysed cells total. **c,**
325 Quantification of HSC daughter cell derived sub tree distances. Two-sided Mann-Whitney test. n
326 = 4 independent experiments. **d,** Paired daughter cell colony assay. HSCs were imaged
327 continuously until after division, then daughters were separated into 96 well plates, cultured for 12
328 days and progeny analyzed by flow cytometry. Quantification of daughter colony similarities
329 across multiple lineages (distance) shows that asymmetric lysosome inheritance predicts daughter
330 cell colony output heterogeneity. n = 5 independent experiments with 37 asymmetric and 32
331 symmetric divisions. Two-sided Mann-Whitney test. Box-plot elements: center line, median; box
332 limits, upper and lower quartiles; Tukey's 1,5x interquartile range; points, outlier.

333 **Methods**

334

335 **Data reporting.** No statistical methods were used to predetermine sample size. The experiments
336 were not randomized and the investigators were not blinded to allocation during experiments and
337 outcome assessment.

338

339 **Ethical statement.** All experiments were done according to Swiss federal law and institutional
340 guidelines of ETH Zurich, approved by local animal ethics committee Basel-Stadt (approval
341 number 2655) and Regierung von Oberbayern (AZ55.1-2-54-2531-59-08)

342

343 **Mice.** Experiments were conducted with 12-16 week old, male C57BL/6J from Janvier Labs
344 (Saint-Berthevin, France) or B6;129-Myctm1Slek/J (GFP-c-MYC KI) purchased from The
345 Jackson Laboratory and acclimatized for at least 1 week prior to start of an experiment. Animals
346 were housed in improved hygienic conditions (IHC) in individually ventilated cages (IVCs) with
347 2-5 animals per cage and supplied with environmental enrichment. Animals were housed with an
348 inverse 12 h day-night cycle in a temperature (21±2°C) and humidity (55±10%) controlled room
349 with ad libitum access to standard diet and drinking water at all times. General well-being of the
350 animals was routinely monitored by animal facility caretakers by daily visual inspections. Animals
351 were euthanized if symptoms of pain and/or distress were observed. Animals were randomly
352 assigned to experimental groups and pooled for experiments to reduce biological variability.

353

354 **Genotyping.** GFP-c-MYC KI mice were homozygous and GFP expression was verified every
355 other generation by flow cytometry.

356 **Cell lines.** OP9 were a gift from Shin-Ichi Nishikawa and cultured in αMEM supplemented with
357 20% fetal calf serum (FCS), 50 U/mL penicillin and 50 µg/mL Streptomycin at 37°C, 5% CO_2.
358 7F2 (ATCC® CRL-12557™) were cultured in αMEM (2 mM L-glutamine and 1mM sodium
359 pyruvate without ribonucleosides and deoxyribonucleosides) with 10% FCS (ATCC, 302020).
360 Cell lines were kept sub confluent and passaged every 2-4 days.
361
362 **Lentivirus production and transduction.** CD53 (imagene, accession number BC052905.1,
363 NCBI), CD63 (accession number BC012212.1, NCBI), Cytochrome c oxidase subunit 8A
364 (COX8a) (accession number NG_046750.1, NCBI), FYVE domain of Sara (imagene, accession
365 number BC032680.1, NCBI), Inscuteable (imagene, accession number DQ205645.1, NCBI),
366 Inturned (accession number NM_175515.5, NCBI), Inversin (gift from Hamada lab, in Osaka
367 University, accession number NM_010569.4, NCBI), Lamp1 (imagene, accession number
368 BC049097.1, NCBI), Musashi-2 (imagene, accession number BC111809.1, NCBI), Numb (p72
369 isoform, accession number AF169192.1), Prkcζ (imagene, accession number BC139761.1,
370 NCBI), Prkcι (imagene, accession number BC021630.1, NCBI), Prominin-1 (accession number
371 BC028286.1, NCBI) and TGFβRI (imagene, accession number BC063260.1, NCBI). cDNAs were
372 cloned into Vesicular stomatitis virus glycoprotein (VSV-G) pseudo typed lentivirus (3rd
373 generation) constructs as either a C-terminal VENUS, N-terminal mCherry fusion or as double
374 fluorescence reporter conjugated GFPmCherry or DsRedpHLuorin as indicated. The virus was
375 produced in Human Embryonic Kidney 293T cells, titrated using NIH-3T3 fibroblasts,
376 concentrated using ultracentrifugation at 68,000 g, stored at -80°C and used at multiplicity of
377 infection (MOI) of 300. Cells were infected for 24 h in 96 round bottom well plates containing

378 IMDM supplemented with 20% BIT, 100 ng/mL SCF, 100 ng/mL TPO, 50 µM 2-
379 mercaptoethanol, 2 mM L-glutamine and 50 U/mL penicillin and 50 µg/mL Streptomycin.
380
381 **Hematopoietic stem and progenitor cell isolation.** Primary cells were isolated and sorted as
382 previously described[22,31]. Briefly, femurs, tibiae, coxae, humeri, ulnae and vertebrae were isolated
383 and crushed in PBS (2% FCS, 2 mM EDTA) and filtered through a 100 µm nylon mesh.
384 Erythrocytes were lysed for 3 min on ice in ACK lysing buffer (Lonza), stained with biotinylated
385 lineage antibodies against CD3ε (145-2C11), CD19 (eBio1D3), TER-119 (TER-119), B220 (RA3-
386 6B2), Ly-6G (RB6-8C5) and CD11b (M1/70), labelled with streptavidin conjugated magnetic
387 beads (Roti®-MagBeads, Roche). After immuno-magnetic depletion cells were stained with anti-
388 CD34-eFluor450 (RAM34), Sca1-PerCP-Cy5.5 (D7), CD48-APC (HM48-1), cKit-PE-Cy7 (2B8),
389 streptavidin-APCeFluor780 (all eBioscience), CD135-PE-CF594 (A2F10.1; BD) and CD150-PE
390 (TC15-12F12.2; Biolegend) for 90 minutes on ice and sorted using BD FACS Aria I or III with 70
391 µm nozzle, single cell purity mode and sorting purities ≥ 98%.
392
393 **Hematopoietic co-cultures.** HSC were cultured as previously described[3]. Briefly, HSC were
394 added in IMDM supplemented with 2% FCS, 30 ng/mL SCF, 30 ng/mL Flt3L, 50 µM 2-
395 mercaptoethanol, 2 mM L-Glutamine and 50 U/mL penicillin and 50 µg/mL Streptomycin to
396 confluent OP9 and 7F2 layer and allowed to settle for 30 min prior to imaging.
397
398 **Stroma free hematopoietic cell cultures.** HSPCs were cultured as described[12,32,33]. Briefly,
399 phenol red free IMDM supplemented with 20% BIT (Stemcell Technologies), 100 ng/mL mouse
400 SCF, 100 ng/mL mouse TPO (both PeproTech), 2 mM L-Glutamine, 50 µM 2-mercaptoethanol,

401 50 U/mL penicillin and 50 µg/mL Streptomycin supplemented with directly conjugated in culture
402 live antibodies or fluorescence probes for quantitative image cytometry: 20 ng/mL CD48-PE
403 (HM48-1), 20 ng/mL CD48-APC (HM48-1), 20 ng/mL CD71-PE (RI7 217.1.4), 20 ng/mL CD71-
404 APC (RI7 217.1.4), 20 ng/mL NOTCH1-PE (22E5, all eBioscience), 50 ng/mL Sca1-Alexa
405 Fluor® 488 (D7), 50 ng/mL CD105-Alexa Fluor 488 (MJ7/18), 20 ng/mL CD41-PE, 20 ng/mL
406 CD41-APC (both: MWReg20), 40 ng/mL CD16/32-BV480 (2.4G2, all BD), 100 nM
407 Tetramethylrhodamine, Methyl Ester, Perchlorate (TMRM, LifeTechnologies), 100 nM
408 CellROX™ Deep Red (Thermo Fisher).
409
410 **Immunofluorescence.** Cells were fixed on either with 100 µg/mL retronectin (Takara Bio) coated
411 or 10 µg/mL anti-CD43-biotin coated slides for 20 min at room temperature with 4% p-
412 formaldehyde (Sigma), permeabilized with 0.2% Triton-X (Applichem), blocked for 1 h in 10%
413 donkey serum in TBS-T (Tris-buffered saline, 0.1% Tween 20) and stained with 4 µg/mL mouse
414 anti-NUMB (Santa Cruz, 48), 4 µg/mL rabbit anti-PARD3b (Santa Cruz, F-12), 2 µg/mL cMYC-
415 Alexa Fluor488 (Santa Cruz, 9E10), 4 µg/mL anti-TOMM20-Alexa Fluor488 (abcam, ab205486),
416 4 µg/mL anti-TOMM20-Alexa Fluor555 (abcam, ab221292), 4 µg/mL anti-LC3β-Alexa Fluor488
417 (abcam, ab225382), 20 µg/mL mouse anti-mCherry (abcam, ab167453), 20 µg/mL rabbit anti-
418 NUMB (abcam, ab14140), 20 µg/mL goat anti-NUMB (abcam, ab4147), 4 µg/mL goat anti-
419 NUMB (Santa Cruz, P-20), 4 µg/mL rabbit anti-NUMB (Santa Cruz, H-70), 4 µg/mL mouse anti-
420 NUMB (Santa Cruz, 48), 2.5 µg/mL mouse anti-alpha-Adaptin (abcam, ab2730), 5 µg/mL rabbit
421 anti-LAMP2 (abcam, ab37024), 1 µg/mL anti-α-Tubulin-AlexaFluor488 conjugate (Life
422 Technologies, B-5-1-2), 100 ng/mL rabbit anti-α-Tubulin-Alexa Fluor647 (Cell Signaling,
423 11H10), 10 µg/mL chicken anti-GFP (Aves Lab) primary antibodies in 10% donkey serum in TBS-

424 T overnight at 4 °C, three washing steps of each 5 min and 10 µg/mL Alexa Fluor dyes conjugated
425 donkey secondary antibodies (Invitrogen) for 3 h at room temperature in 10% donkey serum in
426 TBS-T and stained with 1 µg/mL DAPI for 10 minutes at room temperature. Images were acquired
427 either on a Nikon Eclipse Ti-E microscope using a CFI Plan Apo Lambda 20X objective (NA 0.75)
428 or Nikon A1 microscope using the CFI Plan Apo λ 100X Oil objective (NA 1.45). Analysis of
429 mitotic HSPC was conducted after 44 h culture at 37 °C, 5% CO_2 in 96 round bottom plates or
430 IBIDI[VI] channel slides (Ibidi) using phenol red free IMDM supplemented with 20% BIT, 100
431 ng/mL SCF, 100 ng/mL TPO, 2 mM L-Glutamine, 50 µM 2-mercaptoethanol, 50 U/mL penicillin
432 and 50 µg/mL Streptomycin. Fluorescence signals in each daughter cell were quantified after
433 background subtraction based on secondary antibody only controls and manual segmentation using
434 Nikon NIS-Elements. Daughter pairs were manually inspected and excluded from analysis when
435 fluorescence signals of daughter cells were negative or barely above background and sister cell
436 ratios of DAPI or α-Tubulin exceeded a factor 1.5-fold. NUMB localization and inheritance were
437 compared in listed commercially available antibodies (not shown) and yielded comparable results.
438
439 **Colocalization analysis.** Pixel and Voxel colocalization was determined using custom written
440 Matlab scripts after initial image processing and thresholding as described above**.** Briefly, image
441 pixel fluorescence intensities of channels to be compared were vectorized. Pixels negative for
442 DAPI and α-tubulin and pixels with relative fluorescence intensity values <5 were excluded using
443 logical indexing. Pearson correlation coefficients of vectorized data with and without
444 randomization were calculated.
445

446 **Time-lapse imaging.** Time-lapse experiments were conducted at 37 °C, 5% CO_2 on µ-slide VI[0,4]
447 channels slides (IBIDI), either coated with 50 ng/mL fibronectin (Takara Bio) or 10 µg/mL anti-
448 CD43-biotin, in phenol red free IMDM supplemented with 20% BIT, 100 ng/mL SCF, 100 ng/mL
449 TPO, 2 mM L-Glutamine, 50 µM 2-mercaptoethanol and 50 U/mL penicillin, 50 µg/mL
450 Streptomycin using Nikon-Ti Eclipse equipped with linear encoded motorized stage, Orca Flash
451 4.0 V2 (Hamamatsu), and Spectra X fluorescent light source (Lumencor). White light emitted by
452 Spectra X was collimated and used as a transmitted light for bright field illumination via a custom-
453 made motorized mirror controlled by Arduino UNO Rev3 (Arduino). Fluorescent images were
454 acquired using optimized filter sets: eGFP (470/40; 495LP; 525/50), YFP (500/20; 515LP;
455 535/30), mKO2 (546/10; 560LP; 577/25), mCherry (550/32; 585LP; 605/15), Cy5 (620/60;
456 660LP; 700/75; all AHF) to detect GFP/AlexaFluor488, VENUS, PE, mCherry,
457 APC/AlexaFluor647, respectively. Time intervals of bright field and fluorescent image acquisition
458 were chosen to minimize photo toxicity. Images were acquired using 10x CFI Plan Apochromat λ
459 objective (NA 0.45) and 40x CFI Plan Apo λ (NA 0.95). Single-cell tracking and image
460 quantification were performed using self-written software as described[10,11,15,34,35].
461
462 **Image quantification and analyses.** Acquired 16-bit images with 2048x2048 pixel resolution
463 were saved as .png and linearly transformed to 8-bit using channel optimized white points prior to
464 analysis. Bright field images were used for segmentation using fastER[35]. Trained labeling masks
465 were subsequently eroded to reduce segmentation artefacts caused by close cell proximity
466 (Settings: Morphological transformation x = 3, y = 3, op = 2, shape: 2) and subsequently dilated
467 (Settings: dilation 6) to ensure proper segmentation and quantification of the entire cell in all

468 fluorescence channel. Tracking and quantification of fluorescence channels was done as
469 described[11] and analyzed using Matlab 2017a (Mathworks).
470
471 **Calculation of sister cell ratio and production rates.** Sister cell ratios were calculated based on
472 the first time point after cell division by dividing the sum of pixel fluorescence intensities of one
473 daughter cell by the other. Depending on the temporal resolution used for individual experiments
474 quantified sister ratios are based on time points between 5 to 60 min after mitosis. Ratios smaller
475 1 were thereby converted to their reciprocal so that all sister cell ratios were consequently ≥ 1.
476 When the coinheritance of multiple factors was assessed, this conversion was done for all
477 fluorescence channel and plotted to NUMB as reference. In this case, again all NUMB sister ratios
478 were consequently ≥ 1, while sister cell ratio of other fluorescence channel could be < 1. Since
479 ratios below 1 are distorted and cannot be directly compared to ratios >1, these ratios were
480 transformed with –1/x and are therefore all ≤ 1. Sister cell ratios of > 1.5x and < 1.2x were
481 considered as asymmetric and symmetric respectively.
482 Production rates were calculated by dividing the sum of fluorescence intensities at the last time
483 point of a cells life time by the sum of fluorescence intensities at the first time point of its cell life
484 time directly after division. It represents in other words the fold increase of the total fluorescence
485 signal throughout a cell cycle.
486
487 **Time series arithmetic for classification into asymmetric and symmetric daughter cell fates.**
488 Classification into asymmetric and symmetric paired HSC daughter cells was done by k-medoids
489 clustering based on Euclidean distances using Matlab 2017a. Prior to clustering, fluorescence
490 intensities were z-normalized across all data points of individual replicates. Next, individual time

491 series of daughter cells were normalized to the fluorescence intensities at the first time point after
492 division (=fold change) and 40 time points total using Matlab's spline function. Daughter cell 1
493 and 2 were concatenated, rescaled to an intensity range of 0 to 100 and subsequently treated as one
494 time series of 80 time points total during cluster analysis. In order to avoid reciprocal clusters, all
495 daughter cells with higher mean fluorescence intensities were set to time point 1 to 40 while
496 corresponding daughter cells with lower mean intensities were assigned to time point 41 to 80.
497 The maximum number of clusters was determined by visual inspection and set to 3, representing
498 symmetric, weak asymmetric and clearly asymmetric HSC daughter cell fates. In case of CD105
499 only 2 clearly distinct clusters were found and used for analysis. When effects of mCherryNUMB
500 or LysoBrite inheritance on daughter cell expression dynamics of CD41, CD105, Sca1, CD48 and
501 CD71 were analyzed, daughter cell time series were sorted according to mCherryNUMB
502 inheritance (daughter cell 1 receiving more mCherryNUMB or LysoBrite) at first time point after
503 division prior to concatenation. mCherryNUMB sister ratios of ≥1.8x and ≤1.2x were considered
504 as asymmetric and symmetric inheritance, respectively. LysoBrite sister ratios of ≥1.5x and ≤1.2x
505 were considered as asymmetric and symmetric inheritance, respectively. Please note that the
506 thresholds used to define symmetric and asymmetric inheritance can differ depending on the
507 experimental design and imaging modalities such as choice of fluorescence reporter or
508 fluorochrome and signal to noise ratio.
509
510 **Cell fate assignment onto cell lineage trees.** Clusters for cell fate assignment onto cell lineage
511 trees were generated based on quantifications of single-cell dynamics (for complete list see
512 Extended Data Figs. 9b-c) and dimensionality reduction using Uniform Manifold Approximation
513 and Projection (UMAP) (metric: Euclidean, neighbors: 4, minimum distance: 0)

514 (https://github.com/lmcinnes/umap.git) and Python. After dimensional reduction, data was
515 clustered using hierarchical clustering based on Euclidean distance and ward linkage. The number
516 of clusters was set arbitrarily by comparison of clustering results with prior knowledge (FcγR,
517 CD41, Sca1 expression levels), homogeneity of parameter distribution within clusters and by
518 reproducibility of cluster frequencies between replicates. The analysis was conducted for a range
519 of predefined clusters which gave comparable results within a narrow range around a total cluster
520 number of 11. Clusters were then assigned to cell lineage trees and cluster frequencies after a-
521 /symmetric LysoBrite inheritance quantified for every generation. Apoptotic cells were excluded
522 from cluster analysis and are not displayed.
523
524 **Calculation of subtree distances.** Subtree distances were calculated based on quantifications of
525 single-cell dynamics. Quantification of single-cell dynamics (i.e. fluorescence intensities of first
526 time point, last time point, mean etc. of time series) were concatenated to a single vector per cells.
527 The Euclidean distance between all cells of different subtrees was then calculated in all
528 permutations across all parameters and the minimal sum of all non-redundant cell-cell comparisons
529 between subtrees determined as subtree distance.
530
531 **Continuous quantitative image cytometry.** Segmentation masks were created using fastER[35] on
532 brightfield images and used to quantify single cell fluorescence intensities for every time point as
533 described[11]. Objects over 50 pixels in size were considered as living cells. Segmentation results
534 were verified by sampled visual inspection for accuracy and correct classification. Single cell
535 frequencies across time points were calculated based on fluorescence intensity thresholds similar
536 to flow cytometry analysis using Matlab 2017a (Mathworks).

537

538 **Liquid culture colony assay.** Liquid culture colony assays were done as described[33]. Briefly,
539 single hematopoietic stem and progenitor cells were sorted into a 384 well plate (Greiner)
540 containing 20 µL of medium, incubated for 8 days at 37 °C and 5% CO_2, stained with 500 ng/mL
541 anti-F4/80-PE-eFluor610 (BM8, eBioscience), 500 ng/mL anti-Ly6G-BrilliantViolet570 (Ly6G,
542 Biolegend), 1.25 µg/mL anti-CD71-FITC (RI7 217.1.4, eBioscience), 500 ng/mL anti-CD16/32-
543 BrilliantViolet421 (93, BioLegend), c-KIT-APC-eFluor780 (2B8, eBioscience), 500 ng/mL anti-
544 CD41-PE (MWReg20, BD) and 250 ng/mL anti-Ter119-PE-Cy7 (TER-119, eBioscience)
545 antibodies and analyzed using a BD Fortessa and BD FACSDiva software or FlowJo 10 (tree star).

546
547 **Translation activity assay.** Translational activity was measured using Click-iT™ Cell Reaction
548 Buffer Kit (Thermo Fisher) according to manual. Briefly, HSC were cultured in medium
549 supplemented with LysoBriteGreen (AAT Bioquest, Cat No 22643), anti-CD71-PE and imaged
550 continuously on 10 µg/mL anti-CD43 coated IBIDI$^{VI\ 0.4}$ channel slide (Ibidi). After time-lapse
551 imaging 44 h of *in vitro* culture medium was exchanged and cells were incubated for 1 h at 37 °C
552 and 5% CO_2 in medium supplemented with 50 µM O-propargyl-Puromycin (Jena Bioscience).
553 Afterwards cells were fixated with 4% para-formaldehyde, permeabilized, blocked and cross-
554 linked for 30min using the Click-iT reaction buffers and 250 nM AlexaFluor-647-azide (Thermo
555 Fisher). Images were acquired as described above and concatenated as last time point to previously
556 acquired time-lapse video. During analysis HSC daughter time series were binned according to
557 their time since division.

558

559 **Paired Daughter Cell assay.** HSCs were continuously imaged in stroma free hematopoietic cell
560 culture conditions and live-stained with a 1:10^5 dilution of LysoBriteNIR (AAT Bioquest, Cat No

561 22461). After 40-44 h of time-lapse culture daughter cells of HSCs that had only divided once
562 were separated into 96-well round bottom plates (CELLSTAR® 96W Microplate) containing 100
563 µL of liquid culture colony assay medium as described above. HSC daughter cells were cultured
564 for 12 days at 37 °C and 5% CO_2, stained with Live/Dead 7AAD (125 ng/mL), anti-Gr1-PE-Cy7
565 (Ly6G, 500 ng/mL), anti-CD16/32-PerCP-Cy5.5 (93, 500 ng/mL, all BioLegend), anti-CD11b-
566 eFluor450 (M1/70, 500 ng/mL), anti-CD71-FITC (RI7 691 217.1.4, 1.25 µg/mL), anti-c-KIT-
567 APC-eFluor780 (2B8, 500 ng/mL), anti-CD41-APC (MWReg20, 500 ng/mL) and anti-Ter119-PE
568 (TER-119, 250 ng/mL, all eBioscience) antibodies and analyzed using a BD Fortessa and BD
569 FACSDiva software or FlowJo 10 (tree star). LysoBrite HSC daughter cells of >1.5 and <1.1 fold
570 were considered as asymmetric and symmetric inheritance, respectively
571
572 **Statistical analyses.** No statistical methods were used to predetermine sample size. The
573 experiments were not randomized and the investigators were not blinded to allocation during
574 experiments and outcome assessment. Unless otherwise stated, all experiments were repeated as
575 independent replicates ≥3x times. All statistical test used were two-sided. Unless stated differently
576 data was analyzed using two-tailed Mann-Whitney U test. Mean ± standard error of the mean
577 (SEM) are displayed using GraphPad Prism 8, R (3.41) and Matlab 2017a (Mathworks). Box-plot
578 elements are defined as: center line, median; box limits, upper and lower quartiles; Tukey's 1,5x
579 interquartile range; points, outlier. Significance levels: *: $p < 0.05$, **: $p < 0.01$, ***: $p < 0.001$.
580
581 **Data Availability.** Source data for all figure are provided with the paper. The datasets generated
582 during and/or analysed during the current study are available from the corresponding author on
583 reasonable request.

584

585 **Code availability.** Software used for data acquisition of immunostainings and time-lapse imaging
586 is commercially available (NIS-Elements 4.3.1) or published and open sourced (YouScope v.2.1;
587 http://langmo.github.io/youscope/). Software for single cell tracking and fluorescence
588 quantification used in this study is published and open sourced (https://doi.org/10.1038/nbt.3626).
589 Software used for image Segmentation is published and open sourced
590 (https://academic.oup.com/bioinformatics/article/33/13/2020/3045025). Software used for
591 dimensionality reduction using Uniform Manifold Approximation and Projection (UMAP) is
592 published and open sourced (https://github.com/lmcinnes/umap.git). Software used for time series
593 clustering was inspired by (https://github.com/dmattek/shiny-timecourse-inspector). All code is
594 available from the corresponding author on reasonable request.

595

596 31. Ema, H. *et al.* Adult mouse hematopoietic stem cells: purification and single-cell assays.
597 *Nat. Protoc.* **1**, 2979–87 (2006).

598 32. Eilken, H. *et al.* Continuous long- term detection of live cell surface markers by ‘ in
599 culture ’ antibody staining. *Protoc. Exch.* 1–7 (2008). doi:10.1038/protex.2011.205

600 33. Takano, H., Ema, H., Sudo, K. & Nakauchi, H. Asymmetric Division and Lineage
601 Commitment at the Level of Hematopoietic Stem Cells. *J. Exp. Med.* **199**, 295–302
602 (2004).

603 34. Rieger, M. A., Hoppe, P. S., Smejkal, B. M., Eitelhuber, A. C. & Schroeder, T.
604 Hematopoietic Cytokines Can Instruct Lineage Choice. *Science (80-.).* **325**, 217–218
605 (2009).

606 35. Hilsenbeck, O. *et al.* fastER: a user-friendly tool for ultrafast and robust cell segmentation
607 in large-scale microscopy. *Bioinformatics* **33**, 2020–2028 (2017).

608 **Extended data**

609

610 **Extended Data Figure 1 | NUMB is asymmetrically inherited during HSPC divisions.**

611 **a,** Freshly isolated HSCs were transduced with fluorescence fusion reporter constructs for 24h and
612 imaged on OP9 stroma cells. POI protein of interest. **b,** Quantification of sister cell fluorescence
613 intensity differences during first division of HSC on OP9. Sister cell ratio above 1.5x were
614 considered as asymmetric inheritance. CD63VENUS shows clear asymmetric inheritance while
615 all other candidates are not clearly different from VENUS only control. Number of independent
616 experiments (n) and total number of analyzed HSC divisions (Div.) are indicated. Two-sided
617 Fisher's exact test. **c,** Representative video frames of dividing HSCs transduced CD63VENUS.
618 Symmetric and asymmetric inheritance of CD63VENUS can be observed. **d-e,** Representative
619 CD63VENUS and mCherryNUMB fluorescence intensity quantification of HSC daughter cells
620 over time for symmetric (top) and asymmetric (bottom) segregation during division. Fold sister
621 difference early after division are indicated, respectively. Intensity differences between daughter
622 cells can also occur (long) after mitosis and do not necessarily indicate asymmetric inheritance.
623 Reliable classification of asymmetric inheritance requires continuous observation of single cells.
624 Except for the representative example of tree 1, mother cell intensities are omitted to improve
625 presentation. n = 3 independent experiments.

626

627 **Extended Data Figure 2 | NUMB is asymmetrically inherited during HSPC divisions.**

628 **a,** Freshly isolated KSL were sorted, cultured in 100 ng/mL SCF and 100 ng/mL TPO, fixed after
629 44h and stained for DAPI, a-Tubulin and NUMB. α-Tubulin was used to identify mitotic cells. **b,**
630 Representative examples of fixed mitotic KSL with symmetric (top) and asymmetric (bottom)
631 inheritance of endogenous NUMB. Bar charts indicate quantification of NUMB levels in sister
632 cells as indicated. Scale bar 5 µm. **c,** Quantification of endogenous NUMB expression level and
633 sister cell intensity ratios in fixed mitotic KSL. **d,** Examples of different NUMB sister cell
634 differences in fixed mitotic KSL. Differences between sister cells are in general small and below
635 2-fold. Low NUMB expression level biases towards higher sister cell ratios. Thus, NUMB staining
636 alone and arbitrary thresholding are not sufficient to discriminate between technical/biological
637 noise and functional relevant asymmetric inheritance. Spearman's r. n = 16 independent
638 experiments, 974 mitosis total. **e-i,** Correlation of NUMB and DAPI, α-Tubulin, PARD3b and
639 AP2A2 sister cell intensity ratio, respectively. Circles in **e** represent a pair of daughter cells (#1
640 and #2). PARD3b and AP2A2 are coinherited into the same daughter cell as NUMB during
641 asymmetric inheritance. DAPI and α-Tubulin sister cell ratios were used as controls and expected
642 to be inherited equally. n = 7, 7, 4 and 3 independent experiments for DAPI, α-Tubulin, AP2A2
643 and PARD3bm respectively. **j,** Correlation of NUMB sister cell ratios with sister cell size ratio.
644 Asymmetric inheritance of NUMB does not rely on difference in cell size upon division. n = 4
645 independent experiments. **k,** Frequency of coinheritance of NUMB and AP2A2 or PARD3b based
646 on data displayed in **g-i**, Sister ratios of >1.1x for both NUMB and AP2A2, PARD3b, α-Tubulin
647 and DAPI respectively were considered as coinheritance. Coinheritance of DAPI and α-Tubulin
648 were used as control. AP2A2 and PARD3b are coinherited into the same daughter cell as NUMB
649 in mitotic KSL during asymmetric inheritance of NUMB. Mean ± SEM. Two-sided Fisher's exact

650 test. n = 7, 7, 4 and 3 independent experiments for DAPI, α-Tubulin, AP2A2 and PARD3b
651 respectively. **l,** Freshly isolated KSL were sorted, transduced with mCherryNUMB and fixed after
652 44 h of culture. Mitotic cells were identified by α-Tubulin staining. **m,** Representative maximum
653 intensity projections of mitotic KSL stained for endogenous NUMB and either transduced with
654 mCherryNUMB or NUMBVENUS. mCherryNUMB localizes to endosomes as endogenous
655 NUMB (arrow heads). NUMBVENUS localizes mainly to the cell membrane. Images were
656 acquired using a 100x oil immersion objective (NA = 1.4). Scale bar 10 µm. **n,** Representative
657 example of Pearson voxel intensity correlation of endogenous NUMB and mCherryNUMB (left)
658 and NUMBVENUS (right) in fixed mitotic KSL. Pearson's r. n = 2 independent experiments. **o,**
659 Quantification of Pearson voxel intensity correlation across 70 analyzed cells total. The
660 localization of the N-terminal mCherryNUMB fusion correlates better than the C-terminal
661 NUMBVENUS fusion with endogenous NUMB. Randomized voxel intensities were used as
662 control. n = 2 independent experiments with 40 and 30 analyzed cells or cell divisions for
663 mCherryNUMB or NUMBVENUS respectively.
664

665 **Extended Data Figure 3 | Continuous quantification of mCherryNUMB and asymmetric fate**
666 **marker of dividing HSCs and their daughter cells.**
667 **a,** Representative examples of trees based on differential CD71 production of sister cells.
668 Differences in CD71 daughter cell production are frequently associated with asymmetric
669 inheritance of mCherryNUMB. Comparable CD71 daughter production is mostly associated with
670 symmetric inheritance of mCherryNUMB. All examples were selected based on CD71 differences.
671 **b,** Representative examples of continuous simultaneous quantification of mCherryNUMB and
672 CD71 expression dynamics. Daughters receiving less mCherryNUMB later upregulate CD71. **c,**
673 Quantification of CD41, Sca1, CD48, CD105 and CD71 production in HSC daughters. A-
674 /symmetric inheritance was defined as >1.8x / <1.2x mCherryNUMB sister cell ratios,
675 respectively. Asymmetric daughters receiving less mCherryNUMB (white) produce more CD48,
676 CD105 and CD71 than their sisters (black). Comparable CD48, CD105 or CD71 production in
677 symmetric mCherryNUMB daughters. n = 3 independent experiments. Two-sided Mann-Whitney
678 test. Box-plot elements: center line, median; box limits, upper and lower quartiles; Tukey's 1,5x
679 interquartile range; points, outlier. **d-e,** Heatmap and quantification of HSC paired daughter cell
680 expression dynamics of Sca1 (522 cells analyzed), CD105 (186), CD48 (186) and CD41 (522)
681 after symmetric and asymmetric inheritance of mCherryNUMB. Asymmetric and symmetric
682 paired daughter cell fates can be observed after a-/symmetric mCherryNUMB inheritance (for
683 quantification see **e**).
684
685

686 **Extended Data Figure 4 | Differentiation is accompanied by metabolic activation, CD71**
687 **upregulation and downregulation of stem cell markers.**
688 **a,** Representative images of HSC derived colonies (after 2.5 days) stained with fluorescent CD71
689 antibody, and TMRM or CellRox DeepRed (ROS). CD71 low (arrow heads) / high cells express
690 low / high levels of GFP-c-MYC, TMRM and ROS, respectively. n = 3 independent experiments.
691 **b-d,** Correlation of GFP-c-MYC, TMRM and ROS with CD71 production, respectively, in HSCs
692 and daughter cells. Fold changes of >2 were considered as activation. Metabolically inactive
693 freshly isolated HSCs are low for CD71, GFP-c-MYC, TMRM and ROS. HSC daughter cells show
694 correlated upregulation of GFP-c-MYC, TMRM, ROS and CD71. mean ± SEM. n = 6, 3 and 3
695 independent experiments with 141, 162, 179 HSCs and 282, 632 and 356 daughter cells for GFP-
696 c-MYC, TMRM and ROS, respectively. Mean ± SD. Two-sided Fisher´s exact test. Spearman's r.
697 **e,** GFP-c-MYC expression in freshly isolated HSCs and MPP1-5 analyzed by flow cytometry.
698 GFP-c-MYC expression is low in HSCs. MPP1-5 have increased GFP-c-MYC expression levels.
699 n = 3 independent experiments. **f-g,** Representative examples of HSC daughters' fluorescence
700 dynamics quantification. HSC daughters that upregulate CD71, also upregulate GFP-c-MYC and
701 TMRM or ROS. In case of asymmetric CD71 onset, CD71 low daughter cells remain low for GFP-
702 c-MYC, TMRM and ROS. n = 3 independent experiments. **h,** Representative images of HSC
703 derived colony after 4 days. Fixation and immunostaining for cMYC and CD71. Cells with low
704 CD71 expression express low level of GFP-c-MYC (arrow heads). n = 3 independent experiments.
705 **i,** Image cytometric quantification of GFP-c-MYC MFI over time. MPP1-5 upregulate GFP-c-
706 MYC faster than HSC. n = 3 independent experiments, mean ± SEM, error bars and individual
707 data points not displayed for better readability. Data from all cells (without known cell identity) in
708 culture at specific time points. **j,** Image cytometric quantification of ROS in HSC and MPP1-5

709 over time. ROS production increased in differentiated cells. n = 3 independent experiments. mean
710 ± SEM, error bars and individual data points not displayed for better readability. **k,** Image
711 cytometric quantification of mitochondrial activity with TMRM 8 h after video start. n = 4
712 independent experiments. **l,** Image cytometric quantification of CD71 MFI of cells derived from
713 TMRM(high) and TMRM(low) HSC over time. Progeny of HSCs with active mitochondria
714 upregulate CD71 earlier than progeny of HSCs with inactive mitochondria. n = 4 independent
715 experiments, 2060 quantified data points (cells) across 5 measured time points total with 1131
716 TMRM(high) and 929 TMRM(low) HSC analyzed. $p = 5.4x10^{-3}$, $2.7x10^{-3}$ and $4.9x10^{-3}$ for time
717 points 0, 12 and 24h, respectively. mean ± SEM. Two-sided multiple t-tests, false discovery rate
718 corrected q = 0.01 (Benjamini-Yekuteli). **m,** Representative images of HSC derived colonies after
719 3 days. Cells expressing high levels of CD71 (arrow heads) have downregulated Sca1 and partially
720 downregulated CD105. No clear correlation of CD41 and CD71 expression levels. n = 3
721 independent experiments. Scale bar 20 µm. **n,** Representative image cytometric quantification of
722 all segmented cells in culture over time for CD71 expression versus CD41, Sca1 and CD105,
723 respectively. Sca1 and CD105 are downregulated during CD71 upregulation. n = 3 independent
724 experiments. **o,** Image cytometric quantification of MFI CD71, Sca1, CD105 and CD41 expression
725 over time in HSCs. At population average, Sca1 and CD105 are downregulated during CD71
726 upregulation. Mean ± SEM. Error bars and individual data points not shown for better readability.
727 n = 3 independent experiments with 723, 450, 372 and 401 HSC analyzed for CD71, Sca1, CD105
728 and CD41, respectively and $\geq 9.3x10^{5}$ quantified data points (cells) across 96 time points total. **p,**
729 Image cytometric quantification of CD71 MFI over time in HSC, MPP1, MPP2 and MPP3. MPP1-
730 3 upregulate CD71 earlier and stronger than HSC and indicates differentiation. Mean ± SEM. Error
731 bars and individual data points not shown for better readability. n = 3 independent experiments

732 with 528, 519, 543 and 557 analyzed HSC, MPP1, MPP2 and MPP3 respectively with $\geq 4.5 \times 10^6$

733 quantified data points (cells) across 96 time points total. MFI = mean fluorescence intensity. ROS

734 = reactive oxygen species.

735 **Extended Data Figure 5 | Lysosomes are asymmetrically inherited during HSC divisions.**

736 **a,** Freshly isolated HSCs were sorted, transduced with either VENUS or LAMP1VENUS and co-
737 cultured on OP9 stroma cell in 100 ng/mL SCF and TPO. n = 3 independent experiments. **b,**
738 Representative video frames of symmetric and asymmetric inheritance of LAMP1VENUS during
739 HSC divisions. Arrow heads indicate asymmetrically inherited LAMP2. **c,** Quantification of
740 normalized LAMP1VENUS and VENUS sister cell intensity ratio. LAMP1VENUS is
741 asymmetrically inherited during HSC divisions. n = 3 independent experiments with 211 and 92
742 HSC divisions analyzed for VENUS and LAMP1VENUS, respectively. Two-sided Mann-
743 Whitney test. Box-plot elements: center line, median; box limits, upper and lower quartiles;
744 Tukey's 1,5x interquartile range; points, outlier. **d,** Mitotic KSL fixed after 44 h of *in vitro* culture
745 and antibody-stained for lysosomal marker LAMP2. Endogenous lysosomal LAMP2 is
746 asymmetrically inherited (arrow heads). n = 2 independent experiments with 31 mitotic KSL
747 stained total. **e,** Quantification of sister cell ratios of LysoBrite and Sca1 at first time point after
748 division. LysoBrite sister cell ratios above 1.5-fold do not correlate with high Sca1 sister cell ratios.
749 n = 2 independent experiments with 56 analyzed HSC division total. **f,** Quantification of LysoBrite
750 sister cell ratio and CD71 production ratio of HSC daughter cells. CD71 production was defined
751 as ratio of CD71 fluorescence intensity at the last time point of a cell cycle divided by the CD71
752 fluorescence intensity of the first time point at the beginning of the cell cycle directly after division.
753 High LysoBrite sister cell ratio anti-correlate with the CD71 production ratio of HSC daughter
754 cells, the HSC daughter cell receiving less LysoBrite upregulates CD71 and vice versa. Based on
755 a threshold of 1.5-fold LysoBrite sister cell ratio, CD71 levels can be predicted with high
756 probability. n = 4 independent experiments with 350 analyzed HSC divisions total. **g,**
757 Representative examples of continuous simultaneous quantification of LysoBrite and CD71

758 expression dynamics. Daughters receiving less LysoBrite later upregulate CD71. n = 6
759 independent experiments. **h,** Quantification of CD41, Sca1, CD48, CD105 and CD71 production
760 in HSC daughters (colors as in h). A-/symmetric inheritance was defined as >1.5x / <1.2x
761 LysoBrite sister cell ratios, respectively. Asymmetric daughters receiving less LysoBrite (white)
762 produce more CD48, CD105 and CD71 than their sisters (black). Comparable CD48, CD105 or
763 CD71 production in symmetric LysoBrite daughters. n = 3 independent experiments for CD41,
764 Sca1, CD48, CD105, n = 6 for CD71. Two-sided Mann-Whitney test. Box-plot elements: center
765 line, median; box limits, upper and lower quartiles; Tukey's 1,5x interquartile range; points,
766 outlier. **i,** Paired daughter cell fate (Sca1 (244 analyzed cells), CD105 (258), CD48 (258) or CD41
767 (244)) cluster (as defined in Extended Data Figs. 4b-e) frequencies after a-/symmetric LysoBrite
768 inheritance. Mean %. **j,** Heatmap and clustering (top) and cluster frequency (bottom) of paired
769 daughter cell NOTCH1 dynamics after symmetric and asymmetric inheritance of LysoBrite. Each
770 row represents one HSC daughter pair (#1 and #2). Daughter #1 receives more LysoBrite during
771 asymmetric inheritance, which predicts NOTCH1 upregulation. (Bottom left) Mean fluorescence
772 intensities over time of clusters 1 and 2 with 218 and 209 pooled time series, respectively. Mean
773 ± SD. n =3 independent experiments. Number of analyzed paired daughter cells indicated (#). **k,**
774 Quantification of HSC mitotic marker inheritance. NOTCH1, CD71, CD105 are asymmetrically
775 coinherited with lysosome, while Sca1 and CD41 are not. No correlation between cell size and
776 lysosome inheritance observed. n = 3 independent experiments. r: Spearman coefficient.

777 **Extended Data Figure 6 | NUMB and lysosomes colocalize partially and are coinherited.**
778 **a,** Freshly isolated KSL were sorted, cultured in 100 ng/mL SCF and TPO, fixed after 44 h and
779 stained for DAPI, α-Tubulin, NUMB, and LAMP2 as a marker for lysosomes. α-Tubulin was used
780 to identify mitotic cells. **b,** Frequency of NUMB and LAMP2 coinheritance into the same daughter
781 cell based on c-e. Coinheritance of DAPI and α-Tubulin with NUMB were used as control. LAMP2
782 is co-inherited into the same daughter cell as NUMB in fixed mitotic KSL during asymmetric
783 inheritance of NUMB. Mean ± SEM. n = 3 independent experiments with 172 quantified mitotic
784 KSL total. Two-tailed Fisher´s exact test. **c,** Representative images of fixed mitotic KSL showing
785 symmetric (top) and asymmetric (bottom) inheritance of NUMB and LAMP2. NUMB and LAMP2
786 are partially co-localized (arrow heads, see **d** and **e** for quantification) and are co-inherited
787 asymmetrically into one daughter cell (see **b** for quantification). Images were acquired using a
788 100x oil immersion objective (NA = 1.4). Bar charts indicate normalized quantification of NUMB
789 and LAMP2 fluorescence signal in daughter cell 1 and 2, respectively. n = 3 independent
790 experiments. Two-sided Mann-Whitney test. Box-plot elements: center line, median; box limits,
791 upper and lower quartiles; Tukey's 1,5x interquartile range; points, outlier. **f,** Representative
792 example of mitotic KSL with symmetric (top) and asymmetric (bottom) inheritance of
793 mCherryNUMB. mCherryNUMB and LAMP2 co-localize partially and are asymmetrically co-
794 inherited into the same daughter cell (bottom, arrow heads). Images were acquired using a 100x
795 oil immersion obj. (NA = 1.4). Scale bar 5 µm. n = 2 independent experiments. **g-h,** Quantification
796 of 3D voxel co-localization of either endogenous NUMB or mCherryNUMB with LAMP2 in
797 mitotic KSL. Frequency of NUMB or mCherryNUMB and LAMP2 positive voxels of all LAMP2
798 positive voxels is shown and vice versa. Endogenous NUMB and mCherryNUMB co-localize
799 partially with LAMP2. Quantification of randomized voxels of NUMB and LAMP2 and

800 mCherryNUMB and LAMP2 were used as control. n = 2 independent experiments with 30 and 46
801 mitotic KSL total for NUMB/LAMP2 and mCherryNUMB/LAMP2 colocalization, respectively.
802 **i,** Video frames of 3 representative asymmetric HSC divisions showing mCherryNUMB and
803 LysoBrite colocalization (arrows) during mitosis. Sca1-AlexaFluor 488 staining used as a more
804 widely distributed control. Scale bar 10 µm. **j,** Pixel colocalization of mCherryNUMB with
805 LysoBrite and Sca1 in mitotic HSCs, respectively. mCherryNUMB and LysoBrite colocalize
806 strongly. Pearson's r. n = 3 independent experiments. **k,** Quantification of
807 mCherryNUMB/LysoBrite and mCherryNUMB/Sca1 fluorescence intensity correlation and
808 colocalization in mitotic HSCs. Cellular localization of mCherryNUMB and LysoBrite correlate
809 strongly. n = 3 independent experiments, 89 HSC divisions analyzed. Two-sided Mann-Whitney
810 test. Box-plot elements: center line, median; box limits, upper and lower quartiles; Tukey's 1,5x
811 interquartile range; points, outlier. ns = not significant.

812 **Extended Data Figure 7 | Autophagosomes and mitophagosomes are asymmetrically**
813 **inherited during HSC divisions.**
814 **a,** To test for intra- versus extra-lysosomal localization of NUMB and mitochondria, HSC were
815 transduced with GFP-mCherry double fluorescence fusion reporters for (1) lysosomal outside
816 surface (LAMP1; negative control), (2) autophagosomes (LC3β; positive control), (3) NUMB and
817 (4) mitochondria (COX8a). The differences in maturation time and pH stability between GFP
818 (matures faster, pH instable) and mCherry (matures slower, pH stable) allow the identification of
819 the reporter in nascent (green), mature (yellow) or lysosomal (red) form and their inheritance upon
820 mitosis. **b,** Representative images of GFPmCherryNUMB expressing cells during mitosis.
821 Asymmetric inheritance can be observed in the mCherry and GFP channels. n = 5 independent
822 experiments. Scale bar 5 µm **c,** Quantification mCherry and GFP inheritance.
823 LAMP1GFPmCherry is localized outside the lysosomal lumen and serves as a control (diagonal
824 yellow line, indicative of equal amount of mCherry and GFP signal that is asymmetrically
825 inherited). Nascent and mature asymmetrically inherited GFPmCherryNUMB is mostly outside
826 the lysosome. Autophagosomes and mitochondria are asymmetrically inherited mostly in
827 lysosomes. n = 4, 3, 3 and 3 independent experiments with 236, 132, 183 and 185 analyzed mitosis
828 for lysosomes, NUMB, autophagosomes and mitochondria, respectively.
829

830 **Extended Data Figure 8 | Translational activity precedes CD71 upregulation and is predicted**
831 **by asymmetric inheritance of lysosomes.**
832 **a,** HSCs were imaged in 100 ng/mL SCF and TPO supplemented with LysoBrite and fluorescent
833 anti-CD71. After 44 h, cells were incubated for 1 h with puromycin, fixed and incorporated
834 puromycin into nascent proteins stained to quantify translational activity. **b,** Representative video
835 frames of HSC daughter cells stained with puromycin and CD71. Asymmetric translational activity
836 correlates with asymmetric CD71 upregulation. Scale bar 10 µm. n = 6 independent experiments.
837 **c,** Quantification of asymmetric translational activity and CD71 upregulation in daughter cells
838 fixed at different times after division. Translational (first) and CD71 (later) daughter cell
839 differences increase over time. n = 6 independent experiments. One-way ANOVA. Box-plot
840 elements: center line, median; box limits, upper and lower quartiles; Tukey's 1,5x interquartile
841 range; points, outlier. **d,** Increased translation precedes CD71 upregulation. **e,** Quantification of
842 CD71, translational activity (Puromycin) and LysoBrite inheritance differences between HSC
843 daughter cells. CD71 and translational activity are upregulated in the same daughter cell (Daughter
844 #2) that receives less LysoBrite during mitosis. Daughter cells with symmetric CD71 upregulation,
845 upregulate puromycin symmetrically. n = 6 independent experiments**.** Two-sided Mann-Whitney
846 test. Box-plot elements: center line, median; box limits, upper and lower quartiles; Tukey's 1,5x
847 interquartile range; points, outlier. **f,** Quantification of CD71 upregulation and translational
848 activity after symmetric and asymmetric LysoBrite inheritance and translational activity. CD71
849 and translation are upregulated in the daughter cell asymmetrically inheriting less lysosomes and
850 are upregulated in both daughters after symmetric lysosome inheritance. Two-sided Chi-square
851 test against hypothesis of random distribution of CD71 upregulation and translational activity. n =

852 6 independent experiments, with 155 and 109 analyzed HSC daughter pairs for symmetric and
853 asymmetric LysoBrite and Translational activity.
854

855 **Extended Data Figure 9 | Cell features used for cell state clustering and dynamics**
856 **quantification.**
857 **a,** Clustering of single-cell dynamics **b,** Heatmap overlay of quantification of single-cell dynamics
858 used for clustering and cell fate assignment to cell lineage tree projected onto UMAP. n = 4
859 independent experiments. **c,** Quantification of cell features per cluster. n = 4 independent
860 experiments**.** Box-plot elements: center line, median; box limits, upper and lower quartiles;
861 Tukey's 1,5x interquartile range; points, outlier. **d,** Quantification of cluster frequencies per
862 generation in cell lineage trees after symmetric and asymmetric lysosome inheritance. Later
863 differentiation is heterogeneous. Mean ± SEM. n = 4 independent experiments. **e,** Quantification
864 of HSC daughter cell derived subcolonies. Asymmetric lysosomal inheritance correlates with
865 increased overall heterogeneity in generation 1 but not in later generations. n = 4 independent
866 experiments**.** Box-plot elements: center line, median; box limits, upper and lower quartiles;
867 Tukey's 1,5x interquartile range; points, outlier. **f-g,** Lineage contribution and colony size of paired
868 HSC daughter cell colony assay after 12 days of in vitro culture. n = 5 independent experiments.
869 Two-sided Wilcoxon matched-pairs signed rank test. Box-plot elements: center line, median; box
870 limits, upper and lower quartiles; Tukey's 1,5x interquartile range; points, outlier.
871

872 **Extended Data Figure 10 | Graphical abstract**

873

874

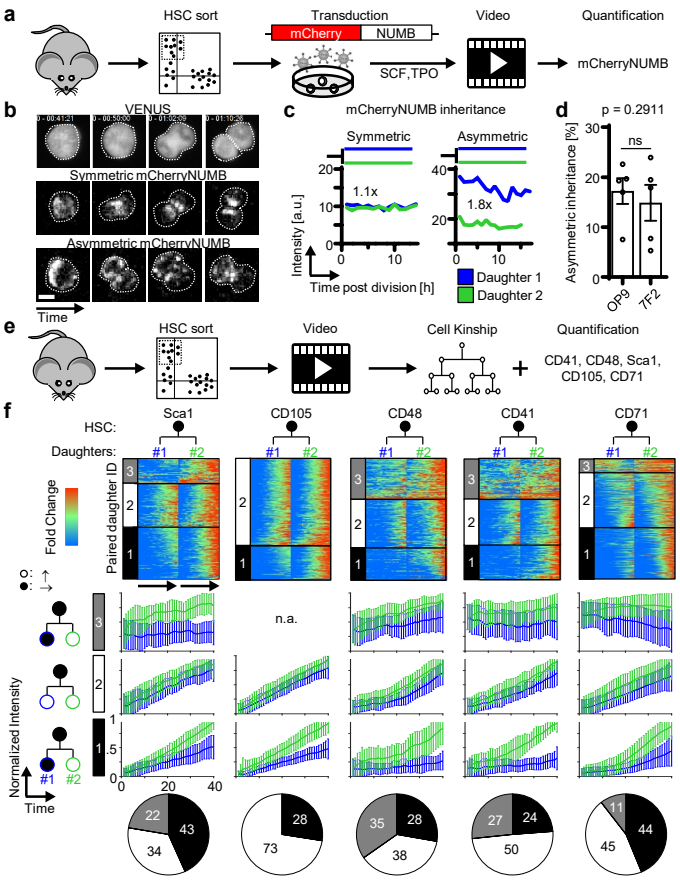

Loeffler et al. Figure 1

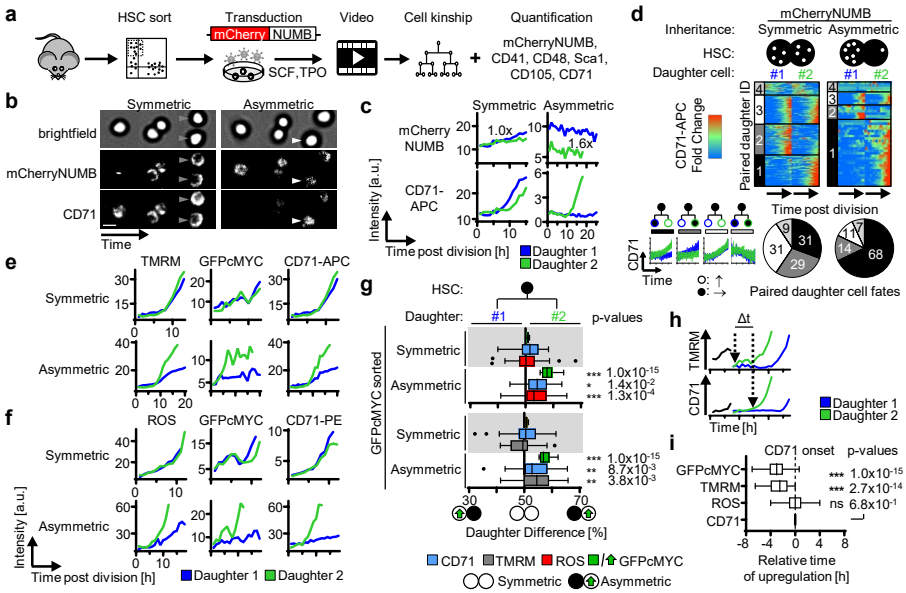

Loeffler et al. Figure 2

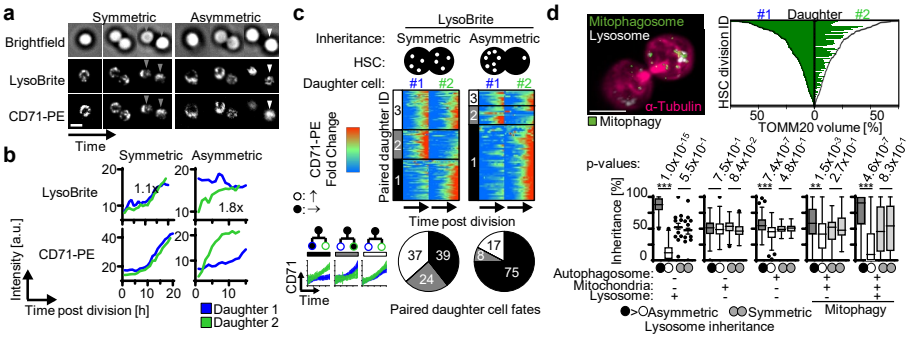

Loeffler et al. Figure 3

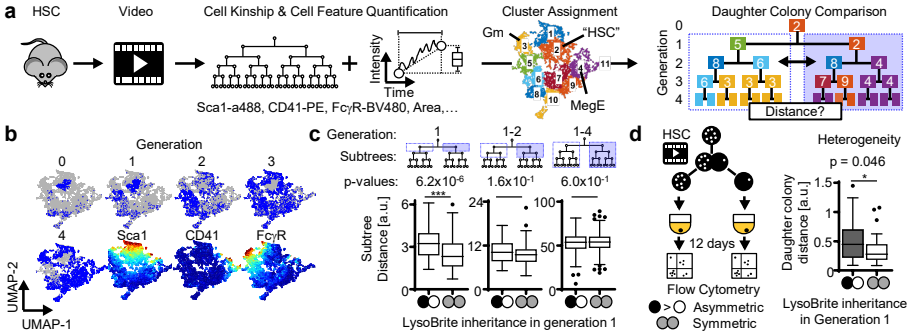

Loeffler et al. Figure 4

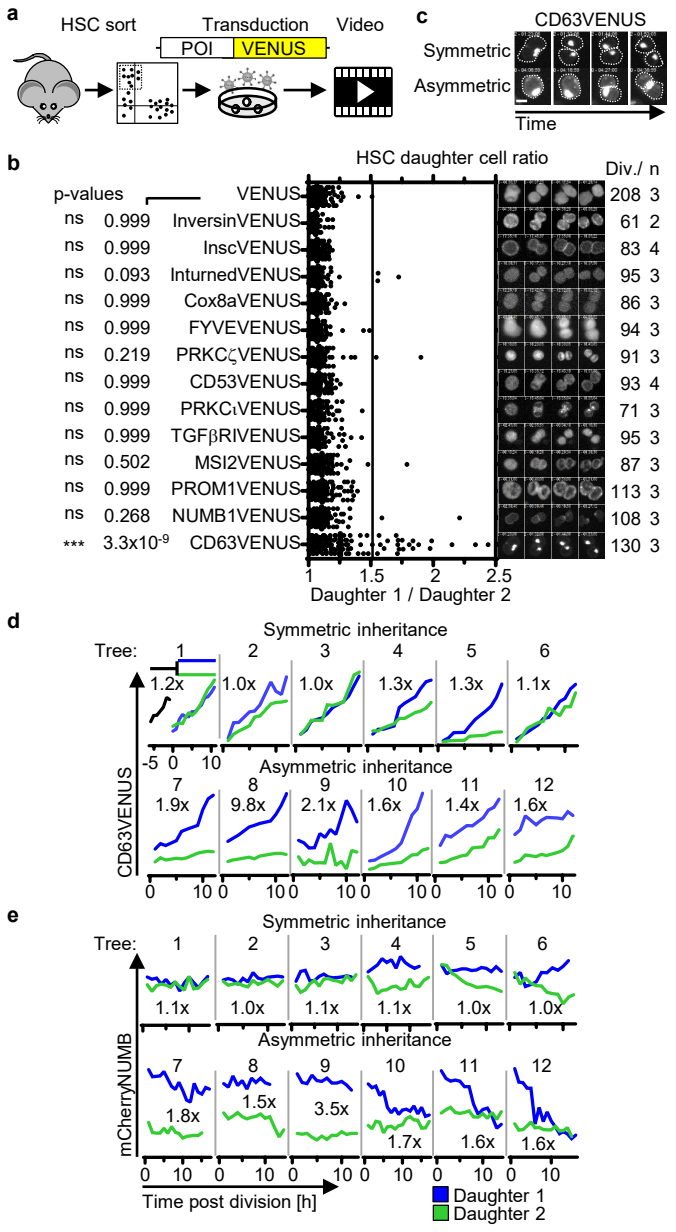

Loeffler et al. Extended Data Figure 1

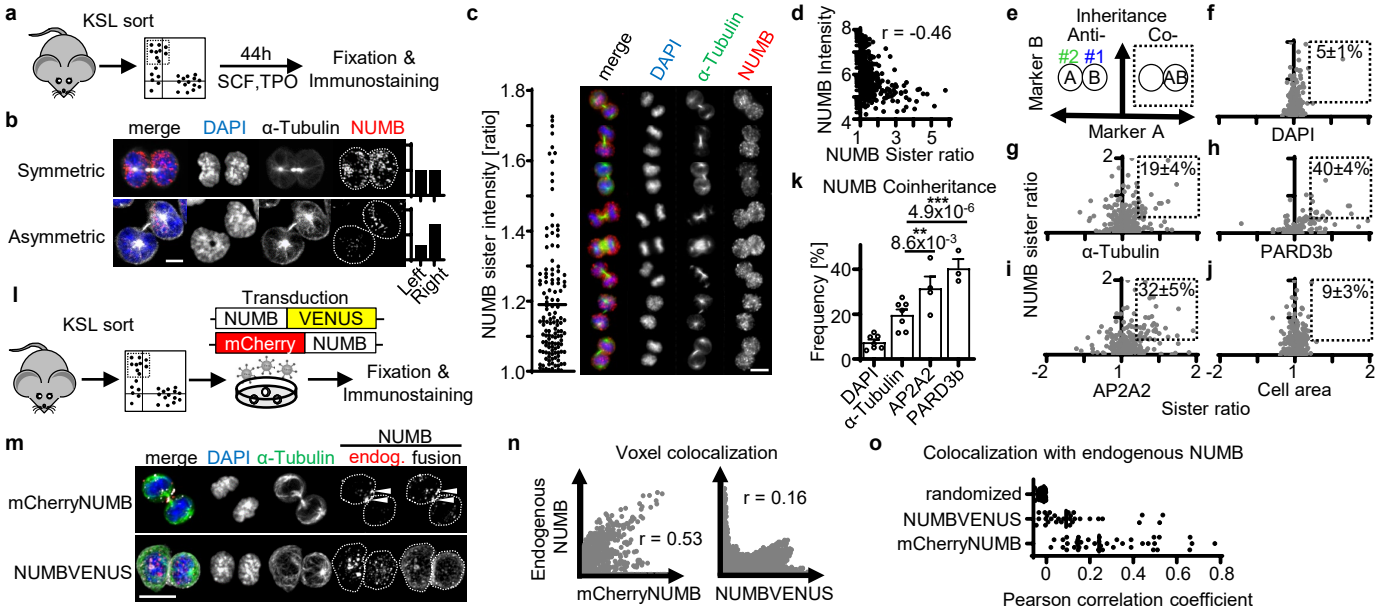

Loeffler et al. Extended Data Figure 2

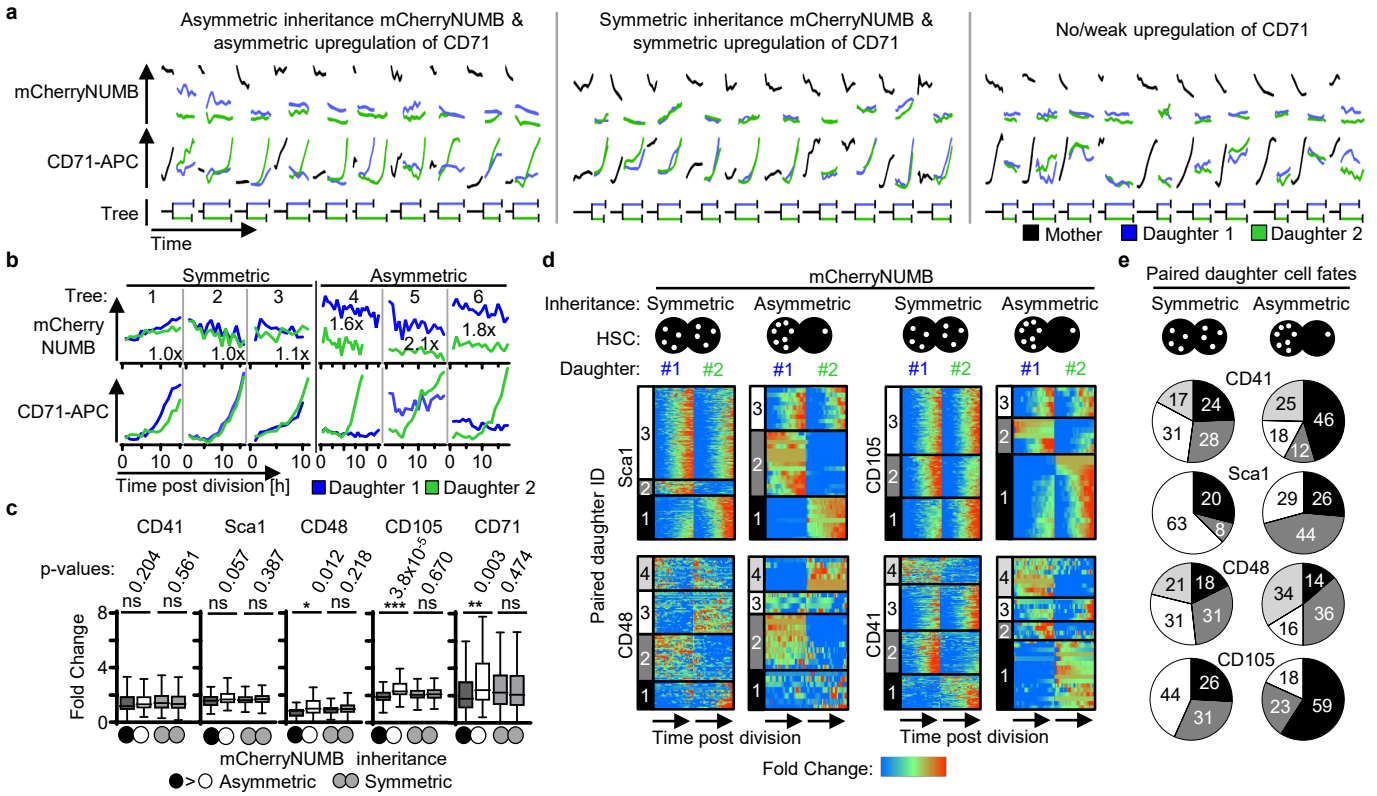

Loeffler et al. Extended Data Figure 3

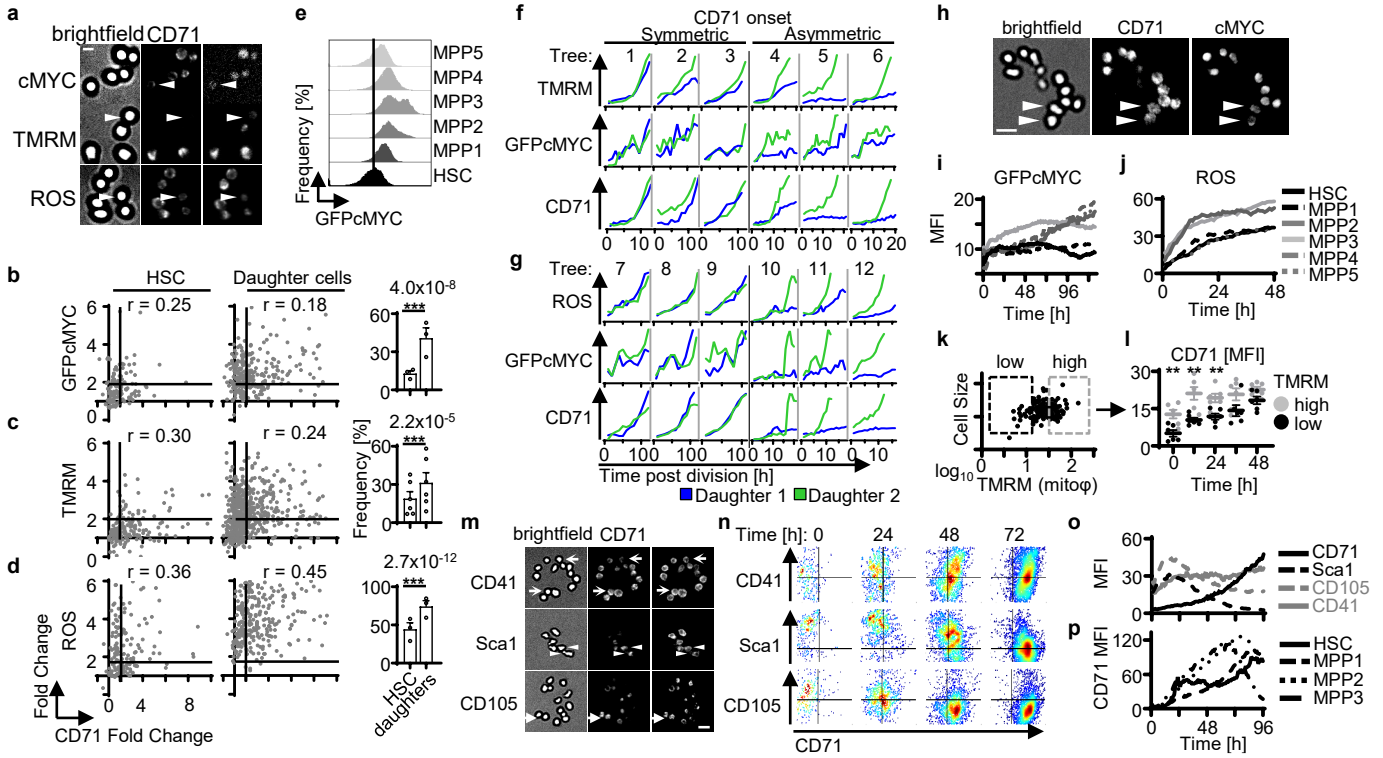

Loeffler et al. Extended Data Figure 4

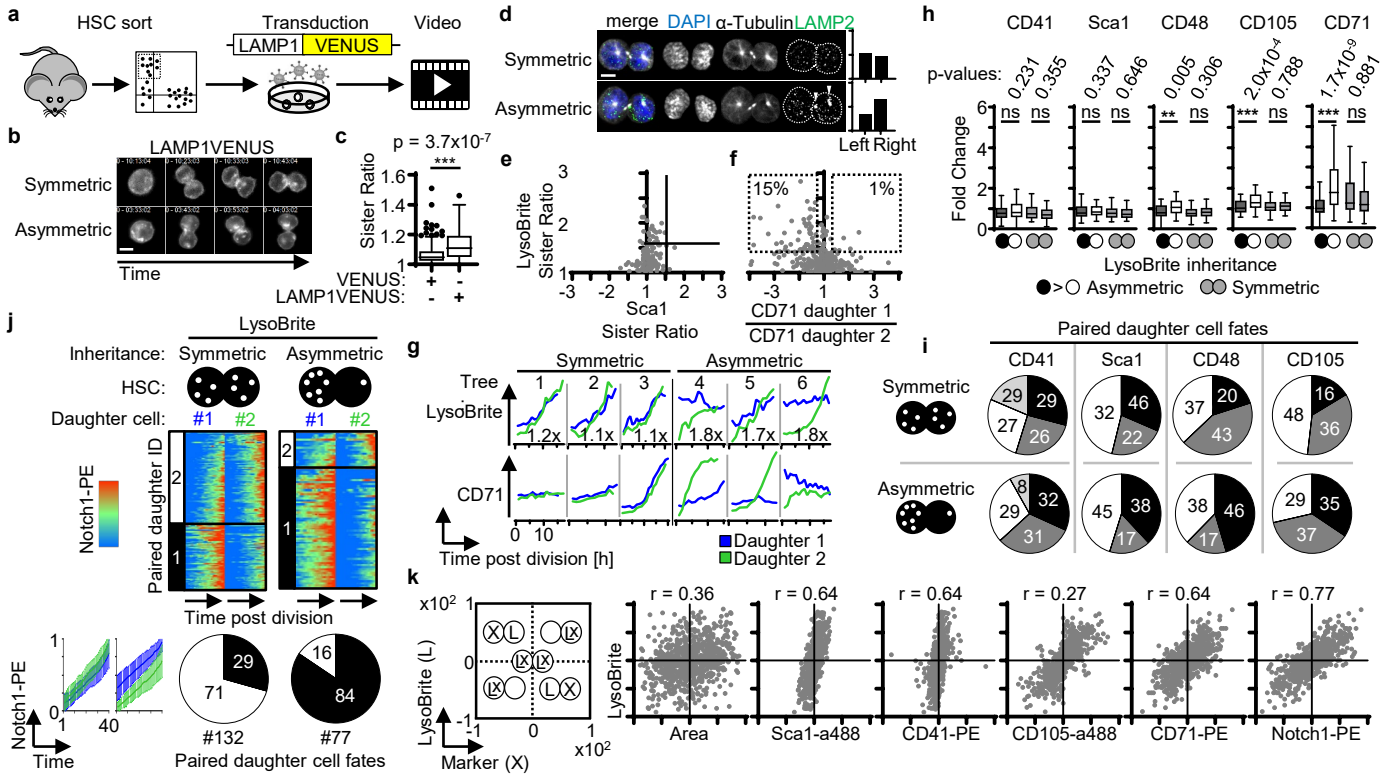

Loeffler et al. Extended Data Figure 5

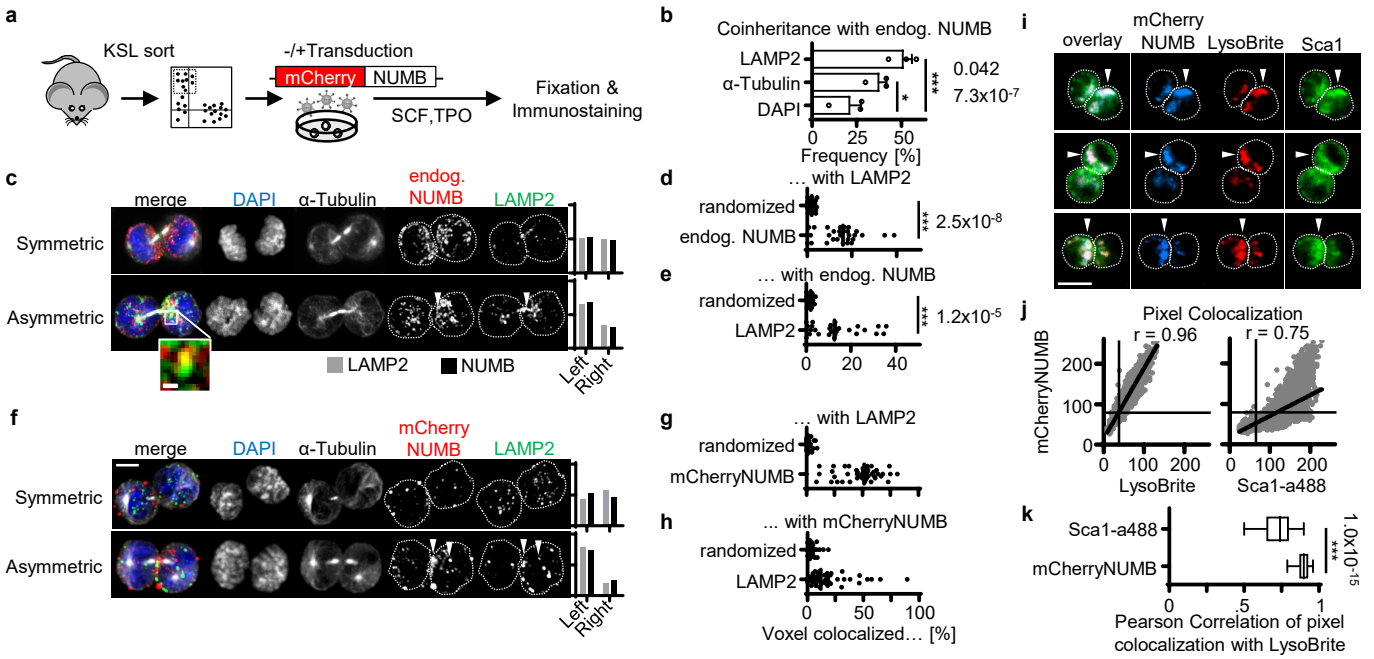

Loeffler et al. Extended Data Figure 6

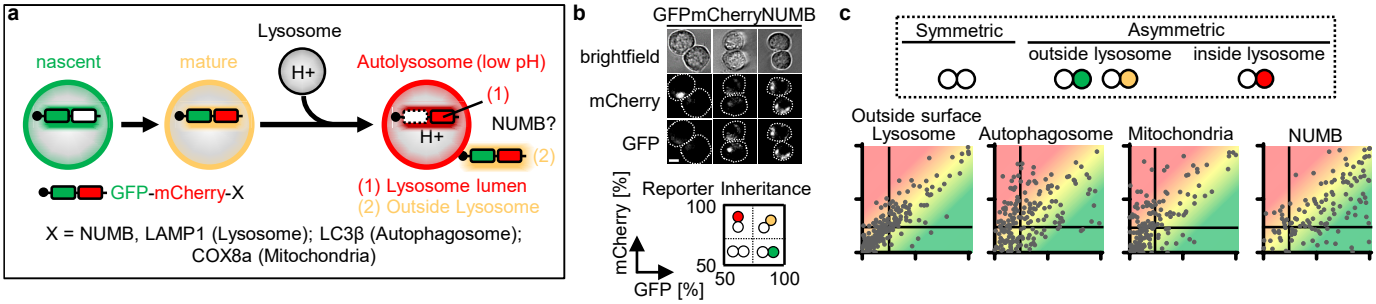

Loeffler et al. Extended Data Figure 7

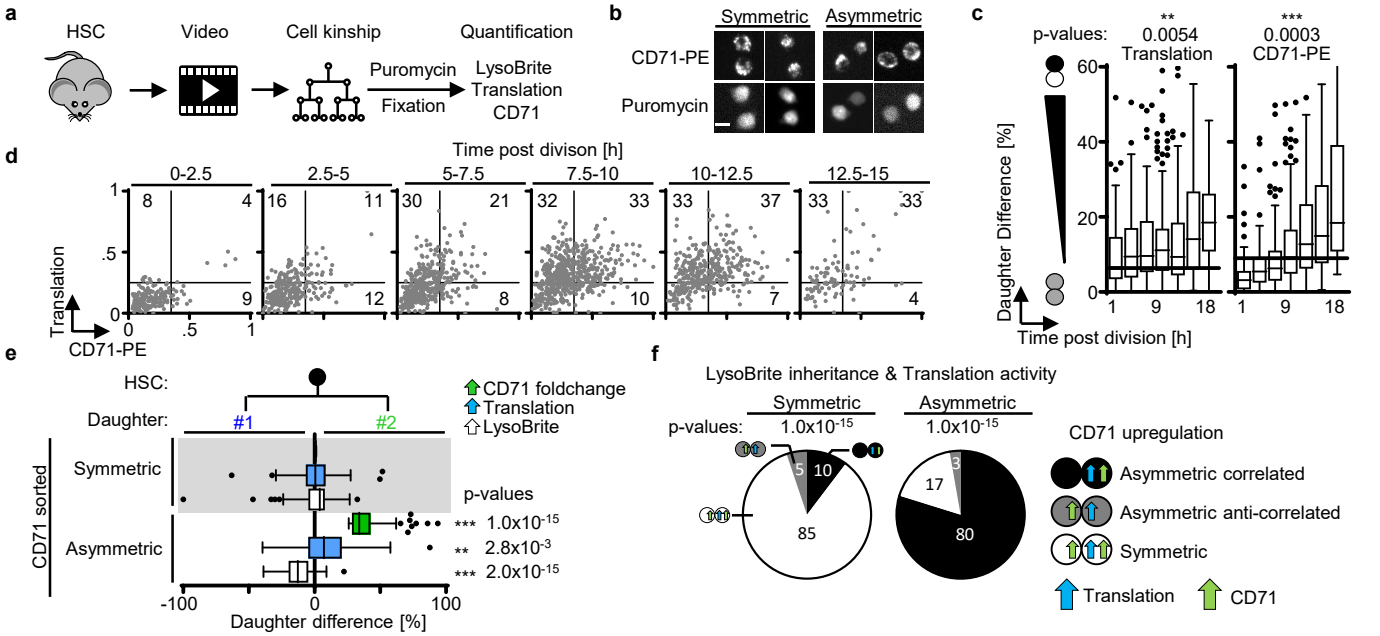

Loeffler et al. Extended Data Figure 8

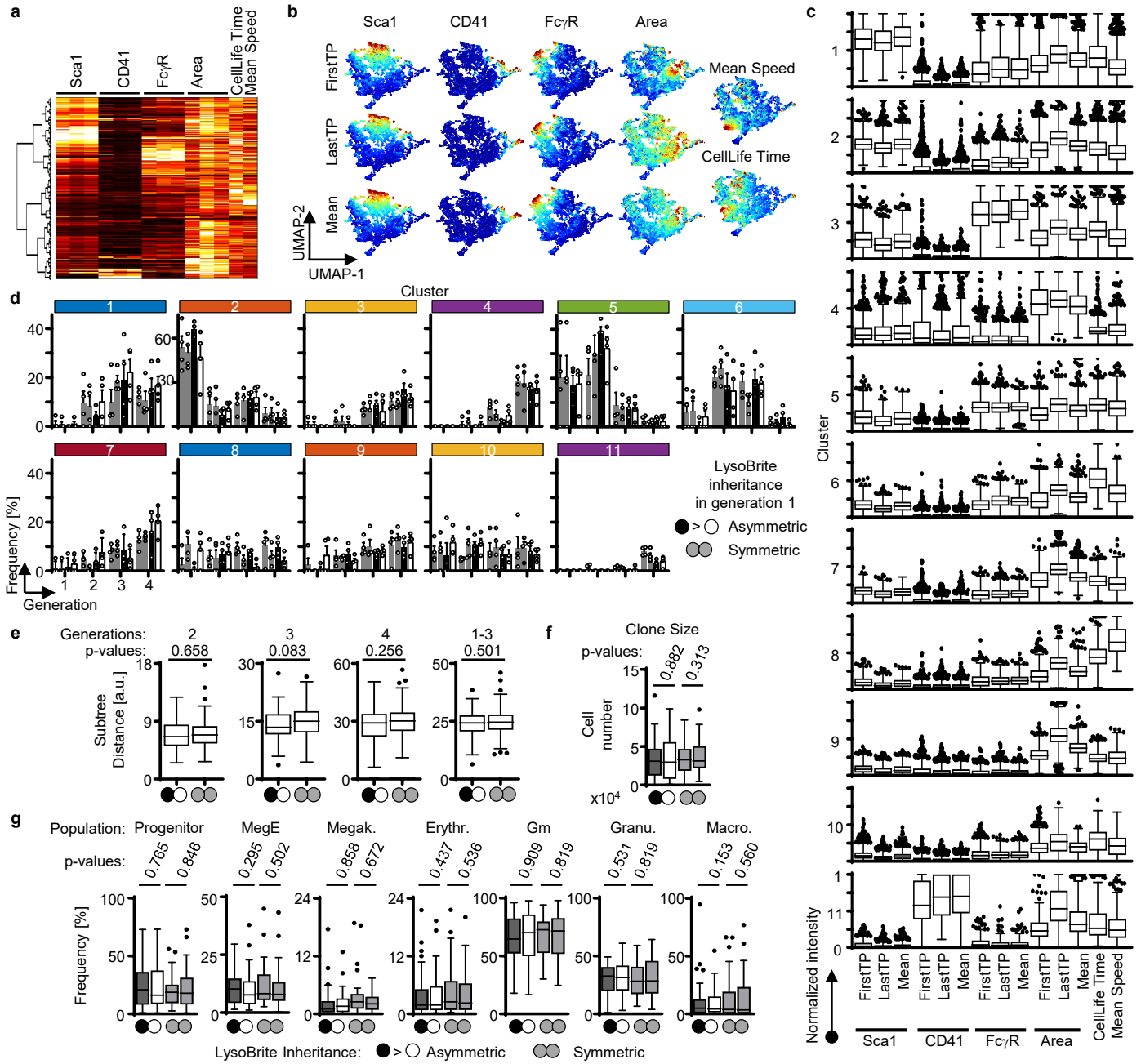

Loeffler et al. Extended Data Figure 9

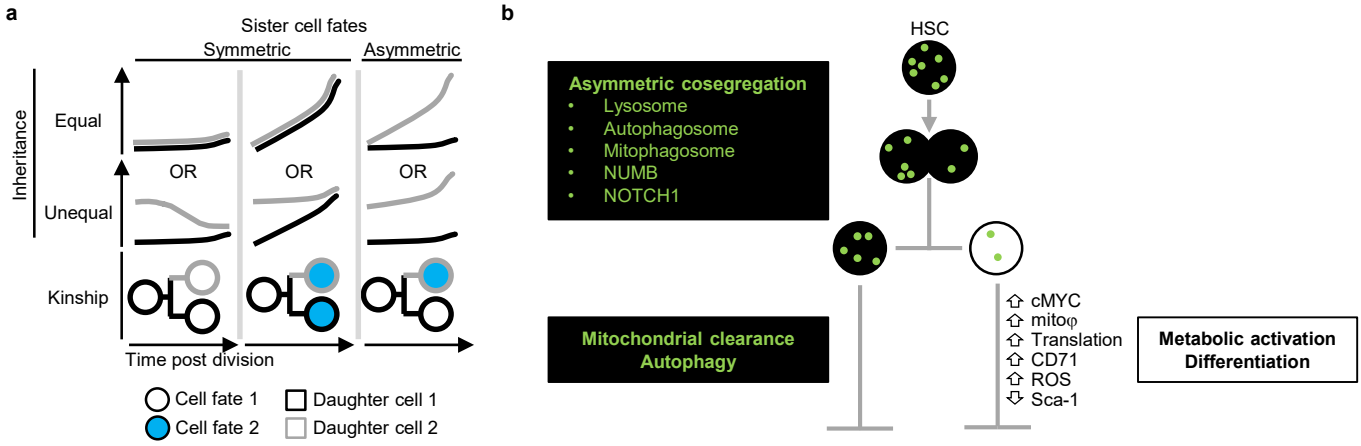

Loeffler et al. Extended Data Figure 10

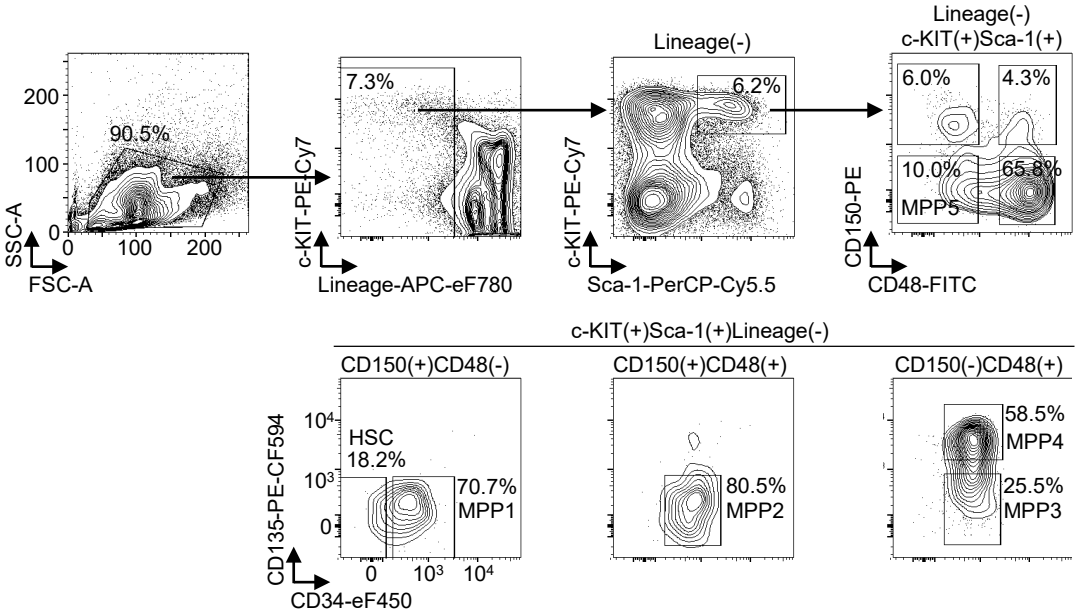

Supplementary Data Figure 1 - Flow cytometric gating strategy for isolation of HSC and MPP1-5s.

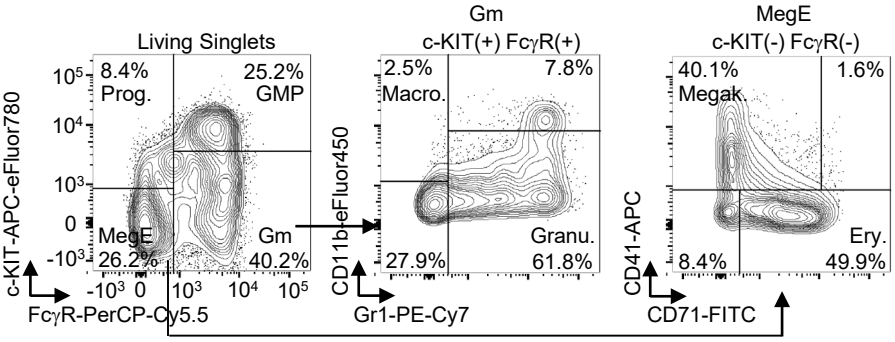

Supplementary Data Figure 2 – Flow cytometric gating strategy used in liquid culture colony assay after paired daughter cell separation